ISSN 1335-8421 Acta Med Mart 2008, 8(2)

ACTA MEDICA MARTINIANA

Journal for Biomedical Sciences, Clinical Medicine and Nursing

Contents

Published by the Jessenius Faculty of Medicine in Martin, Comenius University in Bratislava, Slovakia

Editorial Office:
Acta Medica Martiniana
Jessenius Faculty of Medicine, Comenius University
(Dept. of Physiology)

Malá Hora 4
037 54 Martin
Slovakia

Instructions for authors: http:||www.jfmed.uniba.sk (Acta Medica Martiniana)

Tlač:
P+M Turany

DEFENSIVE AIRWAYS REFLEXES INDUCE WIDELY SPREADING FOS LABELING IN THE CAT BRAINSTEM

IVAN POLIAČEK[1,3], JÁN JAKUŠ[1], ERIKA HALAŠOVÁ[2], HELENA BARÁNI[1], PETER MURÍŇ[1], DONALD C BOLSER[3]

[1]Institute of Medical Biophysics, [2]Institute of Medical Biology, Comenius University Bratislava, Jessenius Faculty of Medicine, Martin, Slovakia, [3]Department of Physiological Sciences, College of Veterinary Medicine, University of Florida, Gainesville, Florida, USA

A b s t r a c t

Fos-like immunoreactivity (FLI) caused by expression of immediate-early gene *c-fos*, a marker of neuronal activation was employed to localize brainstem neuronal populations functionally related to the mechanically induced tracheal-bronchial cough (TBc), aspiration reflex (AR) and expiration reflex (ER). Spontaneously breathing, non-decerebrate, pentobarbital anesthetized cats were used, 6 animals in each stimulated group and 7 control cats. In the **medulla** all 3 reflexes enhanced FLI in the region of *solitary tract nucleus* rostral to the obex (AR-related FLI was also higher than FLI in ER and TBc) as well as in an *intermediate ventral respiratory group*. Increased FLI was found within the region of *retroambigual nucleus* in AR and TBc. FLI within the *most rostral ventrolateral medulla* was higher in TBc and ER (ER-related labeling was also higher compared to that in AR). AR-related FLI was found in the area of the *lateral tegmental field*, in the *caudal solitary tract nucleus* (within both areas FLI was higher also compared to findings in ER), and within the *raphe*. ER-related FLI was also found within the *medullary vestibular area*. In the **pons** FLI was higher within the *area of rostral dorsolateral pons* both in AR and TBc compared to that found in control and ER. FLI in TBc was found in the *posteroventral cochlear nucleus* (higher also compared to FLI in AR). In the caudal **midbrain** FLI was enhanced within the *ventral and lateral periaqueductal gray* in AR (higher also conpared to that in TBc). In TBc and ER FLI mostly diminished within the *lateral periaqueductal gray* (also in comparison with AR-related FLI). Within the *central tegmental field* higher FLI was found in AR and TBc. In the area of the *rostral mesencephalic midline* FLI was increased in ER and TBc compared to that in control and AR. **Our results indicate that:** 1) a complex multilevel neuronal network is involved in production of defensive airway reflexes, 2) the areas of rostral ventrolateral medulla and the rostral mesencephalon may contribute to forceful expirations, whereas the medullary tegmental fields, the rostral dorsolateral pons, and the caudal mesencephalon might be involved in strong inspiratory efforts, 3) some of brainstem regions may contain neurons specifically stimulated during particular behavior.

Key words: Fos, aspiration reflex, cough, expiration reflex, cat

INTRODUCTION

Defensive airway reflexes such is the aspiration reflex (AR), cough, expiration reflex (ER), and sneeze serve to protection of the lungs, and thus significantly contribute to physiological functions of the respiratory system (1). Increased or diminished expression of these behaviors markedly affects the respiration, particularly under pathological conditions. Processes involved in airway defensive reflexes have strong influence on the respiratory system, they can alter or even abolish normal ventilation during their execution. Several populations of respiratory neurons are involved in a production of these responses (2, 3, 4, 5). The results of recording (6, 7), lesioning (8, 9, 10), and stimulating (11) experiments suggested an involvement of both the respiratory and non-respiratory neurons in production of these reflex behaviors. Recent view on central control of the reflex airway defense accepts the solitary tract nucleus (NTS) as a primary projection site of afferents from the airway receptors and also as a first stage of central processing of such inputs. It includes several behavioral modifications of the reflex responses being dependent on actual conditions (e.g. a plasticity related to the type of stimulation, arousal, pathological process, etc.; 12). It

A d d r e s s f o r c o r r e s p o n d e n c e :
Poliaček I., Department of Medical Biophysics, Comenius University Bratislava, Jessenius Faculty of Medicine, Malá Hora 4, 03754 Martin, Slovak Republic
E-mail: poliacek@jfmed.uniba.sk, Phone: +421 43 4221422, Fax: +421 43 4222260

seems that defensive airway reflexes (cough, ER, sneeze) could be generated by the same neuronal network located in the rostral ventrolateral medulla (VLM) that is known to produce quiet breathing (4, 5, 13). The motor pattern is transmitted into the respiratory muscles through the premotor and motor neurons (see e.g. 14, 15, 16). Recently, we proposed a hypothesis that multiple areas involved in central control of these behaviors are organized in multilevel, hierarchical, and holarchical neuronal circuits. They perform primarily a "behavioral" control function regulating the expression of individual reflexes (17). We presume that some of thouse control circuits might be dominant and other only modulatory. On the other hand, different stimuli interact to produce optimum responses. Presumptive holarchical organization of behavioral control elements for different reflexes represents the complex system of equal, comunicating, and cooperating components creating new features, which are not present within individual elements of holarchical system (17).

To summarize the brainstem areas contributing to the generation or modulation of the airway reflexes we implemented the *c-fos* immunocytochemical method. We searched for spreading of Fos-like immunoreactivity (FLI) related to AR (18), TBc (19), and ER (20) in order to compare our findings with the *c-fos* studies of Wallois et al. (21) on sneezing and Gestreau et al. (22) on fictive laryngeal coughing (Lc). Detection of Fos-like proteins, products of the expression of immediate early gene *c-fos*, is a sensitive method for detection of transsynaptic neuronal excitation (23,24). Hence, the Fos method may give a picture of the neurons being employed in processing a variety of motor behaviors.

The current study was designed to examine the differences in Fos labeling in the AR, TBc, and ER. In addition, we performed a comparison of responses with forceful inspiratory and/or expiratory efforts taking into account the Fos studies on Lc (22), sneezing (21), and vomiting (25). We hypothesized an existence of brainstem regions that may contain neuronal populations contributing solely to a production of the forceful inspirations and forceful expirations. Also we intended to determine the differences in Fos staining in all of the mentioned above reflexes.

METHODS

Experiments were performed on 25 adult cats of either sex. The animals were divided into four groups. In each stimulated group 6 cats were used in order to induce repetitive ARs (3.02±0.32 kg), repetitive ERs (3.03±0.22 kg), and repetitive tracheal-bronchial coughing (2.90±0.23 kg). The other 7 animals (3.17±0.32 kg) represented a control non-stimulated (sham operated) group. Cats were anesthetized with pentobarbital (Vetbutal, Polfa) by an initial dose of 35-40 mg/kg i.p. The proper level of anesthesia was maintained by a repetitive dose of anesthetic given intravenously (1–3 mg/kg/hour) as needed. Skin and muscle infiltrations were performed by local anesthetics (Mesocaine, Zentiva) at the sites of surgical interventions to minimize induction of *c-fos* due to stimulation of nociceptors (26).

The trachea was cannulated in all animals allowing the cat to breathe and for mechanical stimulation of lower airways (in coughing cats). Catheters were inserted into the right femoral vein and artery in order to inject supplemental doses of anesthetic and for monitoring the arterial blood pressure, respectively. Blood pressure, airflow, tidal volume, and the end-tidal CO_2 concentration were monitored. Then the mean values of respiratory rate, systolic and diastolic blood pressures, and end-tidal CO_2 concentration were taken in the pre-stimulation control, stimulation, and survival time periods (analogously for non-stimulated cats in early-control and late-survival periods). These values did not differ during the course of experiment and between the groups of animals (ANOVA). Immunohistological tissue processing was restricted only to animals that had maintained systolic/diastolic values of blood pressure within the range 120–195 / 65-130 mmHg (16–26 / 8.5–17 kPa), the respiratory rate 13 – 25 breaths / min., and the end-tidal CO_2 concentration between 4% and 6%. Rectal temperature was kept at 36.5–38.5 °C using a heating lamp and a pad.

All 3 reflexes were induced mechanically by a nylon fibre (diameter 0.2-0.35 mm). ARs were induced by tactile stimuli to the nasopharynx through the nose, and were mostly applied at inspiratory period of breathing. AR was depicted as a short inspiratory effort with a sharp negative swing in the airflow curve. Repetitive coughs were obtained from the trachea and large bronchi by continuous stimulation lasting 5–15 s. Cough was characterized as forceful expulsion that immediately followed previous preparatory inspiration. It was detected in the airflow record as a prolonged deep negative (inspiratory) wave immediately reversed to a strong positive one. ERs were induced from the glottis by a nylon fibre or nylon loop inserted into the trachea rostrally. ER was characterized as a single, short-lasting, and strong expiratory effort being detected in airflow as a narrow and sharp positive swing. Some "non-stimulating" respiratory cycles and also longer resting periods (1 to 3 min) were allowed for complete recovery of the normal breathing pattern. During the 25-40 min period of stimulation 450±30 (270-520) ARs in the group of 6 animals with AR, 170±12 (140-217) coughs in the 6 coughing cats, and 296±9 (270-320) ERs in 6 cats with ER were induced.

Following the preparatory period (approximately 1 hour from the induction of anesthesia to the completion of surgery), the stimulation protocol was initiated 30 min later. After the stimulation period (25-40 min; control cats were only monitored), all cats had the same 2 hour survival time (23,27), so the perfusion of all animals occurred 3 hours after the completion of the surgical preparation. Animals were then deeply anaesthetized (by an additional dose of 10 mg/kg of pentobarbital i.v.) and perfused transcardially with a 2500 ml bolus of saline containing heparin (1000U/100ml), followed by a solution of 1500 ml of paraformaldehyde 4% in 0.1 M phosphate buffer at pH 7.4. The histochemical procedures were described in detail in our previous reports (18,19,20).

Every fifth brainstem section was processed immunocytochemically for Fos-like proteins, then it was used for identification and counting of FLI neurons (one count every 0.2 mm of rostro-caudal dimension). Anatomical landmarks for detection of brainstem structures were generally established using adjacent counterstained sections. The graphic reconstructions of representative sections were performed according to the cytoarchitectonic atlas (28). The subdivisions of the NTS are referred according to Kalia and Mesulam (29), and that of Berman (28), and Petrovicky (30) for other brainstem structures. The distribution and the number of Fos positive neurons were determined with an optical Leitz microscope and videoscanning system (CCD Philips) coupled to a computer. The counted cells were inspected (and confirmed) for a presence of Fos staining under the high magnification of the microscope. Software Ellipse (ViDiTo) was also used to evaluate the grain density by automatic counting of all dots from the same pre-selected level of intensity. The number of FLI neurons in particular structures was averaged to obtain mean count per each area of brainstem *(the average group number of FLI neurons in particular area/hemisection)*. Individual data were collected for comparison and averaging between the right and left sides of corresponding brainstem structures, and for comparison between differently stimulated and the control groups of cats. All data were processed statistically and are given as a mean ± S.E.M. Analysis of variance (ANOVA) with Student-Newman-Keuls post tests and Kruskal-Wallis test with post tests (Dunn) were used as appropriate for statistical processing. In all cases $p<0.05$ was considered significant.

RESULTS

The reflexes had just little effect on ensuing breathing. Some prolongation of respiratory cycles was typicaly found after the AR or TBc trials (18,19). A slight shortening of the expiratory phase was usually observed during the stimulation of ER (20). The respiratory rate returned to the baseline within 5-20 s after the completion of stimulation. At experiments there was no significant difference in the mean respiratory rate, blood pressure, and end tidal CO_2 concentration during and after stimulation referred to the baseline and compared to the control, sham-operated animals.

Table 1. Unilateral Fos-like immunoreactivity counts

Level (mm)	Nuclei and regions	AGN/H			
to obex		Control	AR	TBc	ER
-4 to -2.5	NRA and adjacent FTL	K 3 ± 1	** 22 ± 3	* 13 ± 3	10 ± 4
	ventral caudal GRC and CUC, most caudal NTS	K 8 ± 1	* 19 ± 1	13 ± 5	12 ± 2
-2 to -1	NRA and adjacent FTL	15 ± 3	** 31 ± 2	* 25 ± 3	++ 18 ± 2
	caudal NTS	17 ± 2	** 40 ± 6	31 ± 6	++ 23 ± 3
0.5 to 2.5	NTS and adjacent 5SP	17 ± 3	*** 93 ± 10	* +++ 45 ± 8	* ++ 47 ± 7
	FTL and medial part of 5SP	K 11 ± 2	** 41 ± 4	20 ± 5	++ 11 ± 2
	Raphe	K 2 ± 1	** 15 ± 3	6 ± 3	3 ± 1
	LRN, NA, NPA	15 ± 4	** 49 ± 11	* 35 ± 7	*** # 65 ± 5
	LRN, NA, NPA, FTL	K 25 ± 5	** 90 ± 11	55 ± 12	* 76 ± 3
3 to 4	NA, NPA, RFN, LRN	K 11 ± 3	** 55 ± 9	* 40 ± 4	* 41 ± 7
4 to 5	VN, dorsal 5SP	K 21 ± 4	32 ± 4	48 ± 17	* 42 ± 4
	RFN, LRN, ventral FTL	15 ± 5	33 ± 10	** 52 ± 8	*** ++ 70 ± 8
	Raphe	K 3 ± 2	* 23 ± 8	12 ± 6	6 ± 4
5 to 6	LRN, caudal VII and RTN, medial IFT, ventral FTL	K 7 ± 3	12 ± 3	* 36 ± 6	** 41 ± 8
	Raphe	K 5 ± 2	* 21 ± 5	21 ± 10	13 ± 4
5.5 to 7	CVP	K 1 ± 1	1 ± 1	** ++ 27 ± 10	6 ± 4
10 to 10.5	BC, COE, NPBM	K 12 ± 3	** 94 ± 6	38 ± 4	++ 13 ± 4
	NPBL, KF	K 11 ± 1	20 ± 3	** 34 ± 5	19 ± 3
	BC, COE, NPBM, NPBL, KF together	23 ± 3	*** 113 ± 7	*** +++ 72 ± 7	+++ ### 32 ± 7
10.5 to 11	BC, COE, NPBM	K 25 ± 4	** 72 ± 10	73 ± 29	35 ± 3
	NPBL, KF	K 79 ± 8	** 266 ± 50	* 179 ± 24	105 ± 14
	BC, COE, NPBM, NPBL, KF together	K 104 ± 7	** 338 ± 59	* 252 ± 49	141 ± 14

12.5 to 14	PAG lateral to AQ	78 ± 15	105 ± 10	** +++ 30 ± 6	** +++ 38 ± 6
	PAG ventral & ventrolateral to AQ	K 51 ± 6	* 79 ± 5	++ 37 ± 8	57 ± 6
	FTC	K 28 ± 3	* 63 ± 6	41 ± 12	51 ± 7
14 to 15.5	FTC	K 11 ± 2	18 ± 5	** 50 ± 18	23 ± 5
17 to 18	midline area	77 ± 9	69 ± 8	* + 114 ± 18	* + 131 ± 11

An average group number of FLI neurons in particular area / hemisection (AGN/H) in brainstem structures for the groups of non-stimulated (Control) cats and the cats with aspiration reflexes (AR), tracheal-bronchial cough (TBc), and expiration reflexes (ER). Four sets of data were compared by ordinary ANOVA or Kruskal-Wallis test with Dunn post tests (K). Statistical significance is shown compared to control (*), to AR (+), and to TBc (#). *,+,#, $p<0.05$; **,++,##, $p<0.01$; ***,+++,###, $p<0.001$; 5SP, parvocellular division of the alaminar spinal trigeminal ncl; AQ, aqueduct; BC, brachium conjunctivum; COE, coeruel ncl.; CUC, caudal division of cuneate ncl.; CVP, posteroventral cochlear ncl.; FTC, central tegmental field of mesencephalon; FTL, medullary lateral tegmental fields; GRC, caudal division of gracile ncl.; IFT, infratrigeminal ncl; KF, Kölliker-Fuse ncl; LRN, lateral reticular ncl; NA, ambigual ncl; NPA, paraambigual ncl; NPBL, lateral parabrachial ncl; NPBM, medial parabrachial ncl.; NRA, retroambigual ncl.; NTS, solitary tract ncl; PAG, periaqueductal grey; RFN, retrofacial ncl; RTN, retrotrapezoid ncl; VII, facial ncl; VN, vestibular nuclei.

Fos-like expression was detected as a dark-brown staining of variable intensity in inspected brainstem slices. Immunostaining in our control animals has been described before (18,19,20). There were no significant differences in FLI found between the left and right hemisections in our animals.

Within the **medulla oblongata** all the studied airway reflexes showed the rise of FLI at rostral extension of NTS (at 0.5-2.5 mm rostral to the obex) and in an intermediate extension of VLM (0.5-4 mm rostral to the obex) including the lateral reticular nucleus (LRN), ncl. ambiguus, ncl. paraambigualis, and the caudal retrofacial ncl. (Table 1, Fig. 1). At the caudal ventral respiratory group (VRG; the area that includes the retroambigual nucleus and an adjacent lateral tegmental field - FTL) Fos labeling was enhanced in AR and TBc, but only slightly and non-significantly in ER (Table 1, Fig. 1). At the most rostral extension of VLM (areas of the retrofacial nucleus, LRN, caudal facial ncl., the retrotrapezoid ncl., and adjacent ventral FTL at 4 to 6 mm rostral to the obex) massive FLI related to TBc and ER was found (Table 1, Fig. 1). Higher FLI counts were detected also within the medullary vestibular area (at 4-5 mm rostral to the obex) in ER. Non-significant increase was found here in TBc (Table 1). AR-related FLI was increased also in the caudal NTS and the ventral caudal gracile. and cuneate nuclei (at 4 to 1 mm caudal to the obex), as well as in FTL with medial edge of parvocellular alaminar spinal trigeminal ncl. (at 0.5-2.5 mm rostral to the obex), and within the rostral medullary raphe (at 0.5-6 mm rostral to the obex; Table 1, Fig. 1). In comparison of the staining related to the individual reflexes AR-related FLI was found significantly higher in rostral NTS compared to both other explored reflexes, in the caudal VRG (at 2 to 1 mm caudal to the obex), in caudal NTS (at 2 to 1 mm caudal to the obex), and in FTL region (at 0.5-2.5 mm rostral to the obex) in comparison with ER. AR induced significantly lower FLI in rostral VLM (at 4-5 mm rostral to the obex) compared to ER (Table 1). At levels 0.5-2.5 mm rostral to the obex ER-related FLI was significantly higher than that one in TBc at the area of VLM (Table 1).

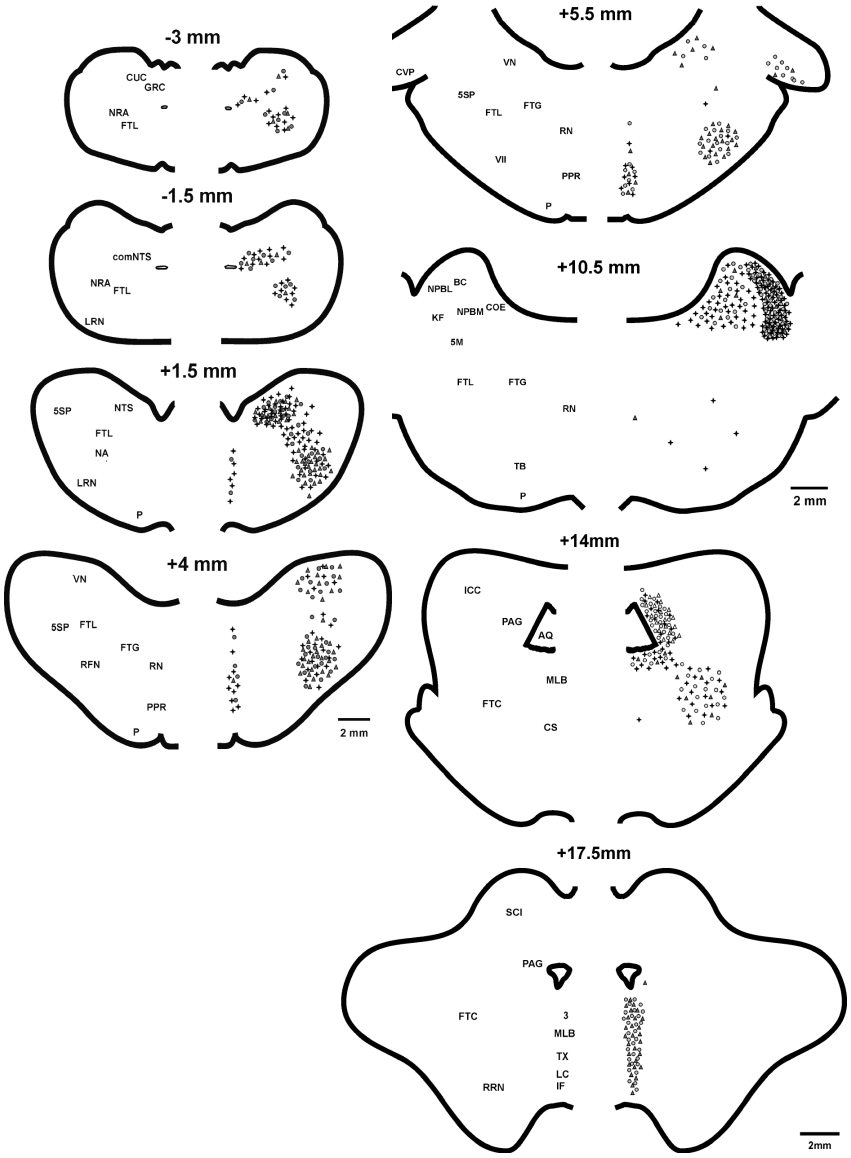

Figure 1. Diagrammatic reconstructions of an augmentation (or reduction) of FLI related to AR, TBc, and ER on transverse brainstem sections. Rostro-caudal extensions are reported in **mm** on the top of each section, -3 and -1.5 caudal, 1.5, 4, 5.5, 10.5, 14, and 17.5 rostral to the obex. An increases in number of stained cells is expressed for aspiration reflex (black stars), for tracheal-bronchial cough (blue circles), and for expiration reflex (red triangels). Decreased number of Fos positive cells is marked for tracheal-bronchial cough (green circles) and for expiration reflex (yellow tringels). Each symbol represent the difference of approximately two Fos labeled neurons in comparison with control (Note: Figures with control staining in our experiments were present in our previous studies: 18,19,20). 3, oculomotor ncl.; 5M, motor trigeminal ncl.; 5SP, alaminar spinal trigeminal ncl.; AQ, aqueduct; BC, brachium conjunctivum; COE, coeruel ncl.; comNTS, commisural subdivision of the solitary tract ncl.; CS, superior central ncl.; CUC, cuneate ncl.; CVP, posteroventral cochlear ncl.; FTC, central tegmental field of the mesencephalon; FTG, medullary and pontine gigantocellular tegmental fields; FTL, medullary and pontine lateral tegmental fields; GRC, gracile ncl.; ICC, central nucleus of the inferior colliculus; IF, interfascicular ncl.; KF, Kölliker–Fuse ncl.; LC, central linear ncl.; LRN, lateral reticular ncl.; MLB, medial longitudinal bundle; NA, ambigual ncl.; NPBL, lateral parabrachial ncl.; NPBM, medial parabrachial ncl.; NRA, retroambigual ncl.; NTS, solitary tract ncl.; P, pyramidal tract; PAG, periaqueductal gray; PPR, postpyramidal ncl.; RFN, retrofacial ncl.; RN, raphe nuclei; RRN, retrorubral ncl.; SCI, superior colliculus; TB, trapezoid body; TX, tegmental decussation; VII, facial ncl.; VN, vestibular nuclei;

Table 2. Semi-quantitative analysis of the neuronal excitation in the brainstem detected by the Fos method during several respiratory-related reflex responses

Area	AR	TBc	Lc	Sneeze	Vom	ER
caudal VRG	+	+	+	+	+	o
caudal NTS	++	o	*	++	+++	o
rostral NTS	+++	++	+++	+++	+++	++
area postrema	o	o	o	o	++	o
trigeminal complex	o	o	o	+++	o	o
intermediate VLM	++	+	+	++	++	+
lateral reticular nucleus	+	+	+	o	o	+
rostral VLM	o	++	++	+	++	++
medullary FTL	++	o	+	+	++	o
medullary FTG	o	o	+	o	+	o
IOM	o	o	*	o	o	o
medullary raphe	+	o	o	o	+	o
medullary vestibular nuclei	o	o	o	o	o	+
pontine FTL	o	o	o	o	++	o
medial structures of PRG	+++	*	+	++	N/A	o
lateral structures of PRG	+++	+++	*	+++	N/A	o
posteroventral cochlear ncl.	o	+	N/A	o	o	o
lateral caudal PAG	o	—	N/A	N/A	N/A	—
ventral caudal PAG	++	o	N/A	N/A	N/A	o
midbrain FTC	++	++	N/A	N/A	N/A	o
rostral midline midbrain structures	o	++	N/A	N/A	N/A	+++

+, significantly increased AGN/H ≥10 cells; *, markedly but non-significantly increased Fos-like immunoreactivity (increase in AGN/H ≥50 cells or increase by more than 200%); ++, significantly increased AGN/H ≥25 cells; +++, significantly increased AGN/H ≥50 cells; —, significantly decreased AGN/H ≤25 cells; the data of other studies were recalculated to 0.04 mm thick sections; N/A, non-available; no counts of the cells and no statistical processing of data is available in study of Miller and Ruggiero (25; the enhancement was estimated from the results reported in the text and from the figures). AGN/H, average group number of immunostained neurons per hemisection; AR, aspiration reflex; ER, expiration reflex; FTC, central tegmental field; FTG, gigantocellular tegmental field; FTL, lateral tegmental field; IOM, medial accessory inferior olive; Lc, fictive laryngeal cough; NTS, solitary tract ncl.; PAG, periaqueductal gray; TBc, tracheal-bronchial cough; VLM, ventrolateral medulla; Vom, vomiting; VRG, ventral respiratory group.

Within the **pons Varolii** a selective TBc labeling was found in the posteroventral cochlear ncl. (the intensity was significantly higher compared to the AR-related FLI as well; Table 1, Fig. 1). In the region of the rostral dorsolateral pons enhanced FLI was found in AR and TBc (Table 1, Fig. 1). It covered primarily the medial structures of the area (brachium conjunctivum, coeruel ncl., medial parabrachial ncl.) for AR and the lateral structures (the lateral parabrachial and Kölliker-Fuse nuclei) for TBc (Fig. 1). At a caudal extension of this region, particularly in the medial structures, the Fos labeling of AR was higher compared to that in ER.

Within the **midbrain** the enhanced FLI was found in the rostral midline area in both TBc and ER (Fig. 1). In both cases FLI was higher compared to AR-related FLI (Table 1). Lower levels of FLI in TBc and ER were found at caudal lateral periaqueductal gray (PAG) when compared to control and also to AR-related FLI. At this extension enhanced Fos labeling was detected within the ventral and ventrolateral PAG in AR (Table 1, Fig. 1). Within the central tegmental field higher FLI counts were observed at levels 12.5-14 mm in AR and at 14-15.5 mm in the case of TBc (Table 1).

DISCUSSION

The major finding of our study was the identification of brainstem areas that contribute solely to the production of forceful expirations vs. inspirations based on statistical analysis of FLI induced by AR, TBc, and ER and also using a semi-quantitative comparison of our data with the results obtained on Lc (22), sneeze (21), and fictive vomiting (25). The brainstem regions, which specifically participate on the analyzed reflexes were exposed as well.

All methodological aspects of our experiments (including the limitations of the method related primarily to the sensitivity and specificity of the Fos labeling; 21,24,31) were discussed in details before (18,19,20). We assume that our results correspond to the FLI induced by neuronal excitation in three studied airway reflexes, analogously as it was stated in another three reflexes being considered here (21,22,25).

Thus, all six evaluated reflexes showed significantly higher counts of Fos positive neurons in the rostral extensions of **NTS** (Table 1 and 2, Fig. 1). Vagal afferents that participate in these reflexes are known to project towards several subnuclei of NTS (29,32,33,34,35). Hence, the higher level of FLI found in the NTS was expected in all of the behaviors. Despite some convergence of inputs, the glossopharyngeal nerve afferents terminate mainly in the rostral two thirds of the NTS, while the vagal nerve afferents (from other airway regions than pharyngeal) target mainly the caudal two thirds of the NTS (34). This fact can explain our findings of significantly higher Fos staining within the rostral NTS in AR compared to TBc and ER (Table 1). Sneeze related Fos labeling was also found in the trigeminal complex in accordance with the fact that signals from nasal nerve afferents target this region as well (21). Afferent inputs that induce vomiting project to the neurons in the area postrema and NTS (36,37) where an intense vomiting-related FLI was found (Table 2; 25). In the areas of NTS rostral to the obex there are clusters of neurons with afferent projections from the pulmonary stretch receptors (35,38). They are also markedly activated by vigorous intrathoracic pressure and lung volume changes in the course of reflexes. Hence, these neurons might contribute to the observed high level of FLI in the area. Most of the afferent information from the tracheal and bronchial rapidly adapting receptors and C-fibers (being acknowledged to trigger the TBc) project to the commisural and the caudal medial subnuclei of NTS (35,39). Relatively high basal staining just below the obex, observed also by Wallois et al. (21) and Gestreau et al. (22) presumably interfered with the level of recruitment of the TBc-related FLI. It may be a reason why we have not detected significantly enhanced FLI related to TBc within the caudal NTS in our experiments (Table 1).

Up-to-date the Fos studies support the concept that the neuronal populations in the main respiratory areas, including respiratory related units (3,4,13), may significantly contribute to the generation and/or to modulation of the airway reflexes. Thus, all areas of **VRG** and even adjacent nuclear and reticular structures were markedly Fos labeled. However, we did not find significantly higher counts of Fos positive cells during ER in the caudal VRG. Similarly, AR-related FLI was not enhanced within the most rostral VLM (Table 1, Fig. 1). The **caudal VRG** (an area of the retroambigual ncl. and adjacent caudal FTL) and the **intermediate VRG** (associated mainly with ncl. ambiguus and paraambigualis) are characterized by populations of respiratory neurons, known to transmit the central respiratory motor drive to the upper airway "valve" muscles and through the spinal motoneurons to the thoraco-

abdominal "pump" muscles (see e.g. 14, 15, 16). The caudal VRG is characterized by a high concentration of expiratory premotor neurons including silent expiratory units that are probably involved in the accretion of the expiratory drive (3,17). Less pronounced ER-related FLI found within the caudal VRG migh be explained by lower number of recruited (5) and excited expiratory units in ER compared to other expulsive behaviors. Also a different shape and a short duration of expiratory activity during ER might be a reason for lower production of Fos immunostaing comparing with coughing, sneezing, or vomiting. However, we found significantly higher level of AR-related Fos labeling in the caudal "expiratory" VRG (Table 1) than that in ER. We speculate, if the medullary premotor units with trajectories to the spinal cord do not respond to their activation with production of Fos (21), similarly as some clusters of motoneurons (21, 40), then FLI being found in caudal VRG may mirror an activity of other not yet specified neuronal populations. Inspiratory units in the caudal VRG are sparse (14, 41) and expiratory activity during AR is generally inhibited (3, 42). Hence, we can not rule out the possibility that the labeled cells found in AR were inhibitory interneurons, which suppress the expiratory units during forceful inspiration. Recently, we presented an evidence for active cough suppressive neuronal mechanism located in the area of caudal VRG (11). It seems that a relatively homogenous "expiratory" pre-motoneuronal area of caudal VRG is much more complex when controlling the expulsive behaviors such is the AR, cough, ER, and sneeze. In contrast, there is a high number of ER-related Fos positive cells in the region of the **intemediate VRG and VLM** (Table 1, Fig. 1). The intermediate VRG is characterized by a functional dominance of inspiratory neurons (see e.g. 14) while a density of expiratory neurons at this region is low. Increased Fos labeling within this region might be explained by activation of inspiratory units during the reflexes with inspiratory component. However, enhanced ER-related FLI found at this region possibly reflects the activity of expiratory units being recruited at the time of ER, since all inspiratory activity during ER is commonly and strongly inhibited (3, 43). If they are either inhibitory interneurons suppressing inspiratory units during the ER or they represent "behavioral control elements" (17) cannot be determined yet. Enhanced FLI was also revealed within LRN during AR, TBc, ER, and Lc (Table 2), however, it was not found in sneezing (21) and vomiting (25). Similarly, more compact Fos labeling, concentrated mainly within the ncl. ambiguus was reported upon laryngeal stimulation inducing laryngeal constriction (44,45). Therefore it is reasonable to suppose that an area of LRN might be specificaly involved in the expression of AR, cough, and ER but not in production of sneeze, vomiting, and laryngeal responses. Since pools of expiratory units in the **rostral VLM** (particularly those from the Bötzinger complex), may provide the excitatory drive to premotor and motor neurons during the cough, ER, and vomiting (5, 46, 47), we assume that higher level of FLI revealed at the rostral VLM may reflect the activation of these expiratory units. It is unknown if also another cells have been activated at this region during TBc, Lc, ER, and vomiting but FLI diffusely covered all rostral VLM reaching even the caudal retrotrapezoid ncl. and adjacent reticular formation including ventrolateral FTL. FLI in this area was never observed following AR (18), and the laryngeal stimulation (44,45). The "expiratory rhythm generator" hypothetically localized in the region of the retrotrapezoid nucleus / parafacial respiratory group (48) may be activated during the active expirations (49,50). The clusters of retrotrapezoid neurons were densely Fos labeled under the hypoxic and hypercapnic conditions (51,52). However, an involvement of these neurons in the expiratory expulsive behaviors such is cough, ER, and sneeze cannot be either proved or excluded on the base of present experiments.

Significantly enhanced Fos labeling in the region of **FTL** was revealed in AR, Lc, sneezing, and vomiting (also in pontine FTL), but not in TBc and ER (Table 1 and 2). There is no natural border between the VLM and the ventral FTL, so some labeled neurons that might be counted in other studies in FTL we could locate within VLM area. Nevertheless, in our experiments AR has shown higher induction of Fos within the FTL than the TBc or ER. Medullary FTL (particularly an area between the NTS and the nucleus ambiguus) was established

as a critical region for fictive gasping (53,54) and the fictive AR in cats (42,55). The reticular neurons in the gigantocellular tegmental field, FTL, and the rostral LRN form a high density of reticulo-nuclear and reticulo-reticular connections with a variety of structures in the medulla, pons and mesencephalon (56). Recording experiments showed the bursts of neuronal activity in FTL and gigantocellular tegmental field during ER (6). However, there was no enhancement of FLI in gigantocellular part of tegmental region and only very limited increase in FLI within FTL during TBc and ER. On the other hand, these areas were stained in Lc and vomiting, too. That is in agreement with a role that could these structures play in vomiting and in the postural adjustments when the inspiratory and expiratory muscles are coactivated (57). Significant increases in number of labeled cells within FTL were reported also after the superior laryngeal nerve stimulation (45).

Among the reflexes just AR and vomiting have induced FLI within the medullary (and pontine) **raphe midline** (Table 1 and 2). Raphe midline is accepted as an important area for control of reflex behaviors such is AR, cough, and ER (7, 8). Significant neuronal pathways from the raphe nuclei connect the NTS and the pontine regions both being involved in control of breathing and the respiratory reflexes (10, 14, 58). However, the scattered Fos labeling within the raphe nuclei suggested only a weak neuronal excitation in cough, ER, and sneeze. Tonically active neurons (including tonic respiratory units) in the raphe (7) may contribute to these reflexes by modulation of their neuronal activity (not inducing FLI).

Unexpected labeling was detected within the posteroventral cochlear ncl. in the cough and within the vestibular nuclei in ER (Table 1, Fig. 1). Similarly, FLI was found in the medial accessory inferior olive for Lc (22). We presume these neurons are not directly involved in processing of the signals related to generation or behavioral control of these reflexes.

The dorsolateral region of the rostral **pons** (an area of pontine respiratory group) contains respiratory units (14). They presumably participate in adaptive reactions serving to the respiratory and cardiovascular systems, particularly to the inspiratory-expiratory transition during breathing (see e.g. 14). Pontine respiratory group neurons are connected with the spinal cord, brainstem, and the forebrain structures (59), e.g. by direct projections from the caudal NTS (60) or from VRG (61). We found an intense Fos labeling related to AR and the TBc in this pontine area (Table 1, Fig. 1). It was also reported for sneeze (21) and in lesser extent for the fictive Lc (22). FLI was more pronounced within lateral structures (the lateral parabrachial and Kölliker-Fuse nuclei; Table 1, Fig. 1) in TBc, or within the medial structures (particularly the medial parabrachial ncl.) in Lc. In sneezing and AR Fos reactivity was massively enhanced at all areas of the pontine respiratory group (Table 1, Fig. 1). Interestingly, we have not detected significant increase in a number of stained cell at that region for ER. Neuronal activation during the defensive airway reflexes within the region of pontine respiratory group (that induces FLI) could be primarily related to forceful inspirations or inspiratory terminations that are absent in ER.

The function of **midbrain** is very complex. Midbrain structures seem to be involved in the modulation of the central respiratory and cardiac sympathetic drives, in changes of the arousal, in somatosensory and alimentary functions, behavioral reactions, in vocalization, etc. (14,62,63,64). The midbrain, particularly PAG and the central tegmental field are connected with NTS and VLM (65,66,67), PAG also with LRN (68). The involvement of midbrain neurons in expression of AR was presumed earlier (9). Hence, the AR related FLI in caudal mesencephalon (ventrolateral PAG and central tegmental field) was not a surprise. (Table 1, Fig. 1). Ambalavanar et al. (69) reported in cats an increase of FLI predominantly within the lateral subdivision of PAG after the superior laryngeal nerve stimulation and the laryngeal adduction. However, in our experiments laryngeal stimulation (and ERs) has induced a less intense Fos labeling within the lateral PAG compared to the control. The reason for this disparity is not known. It is of interest that also TBc-related FLI at this region was diminished (Fig. 1) and both TBc and ER related FLIs were significantly lower than that one for AR (Table 1). Central tegmental field of the mesencephalon expressed enhanced FLI in TBc, similarly as in AR, however, at different rostro-caudal extensions (Table 1). We reve-

aled a higher level of Fos staining within the structures of the rostral midbrain midline in TBc and ER that was significantly higher when comparing with the FLI in AR (Table 1, Fig. 1). Contribution of the neurons located at mesencephalon to the control of airway reflexes remains obscure.

Conclusions. The Fos method showed widely spread neuronal excitation suggesting that a complex multilevel brainstem neuronal networks are involved in production of respiratory related reflexes. Statistical analysis of the number of Fos positive neurons in AR, TBc, and ER along with a semi-quantitative analysis of FLI in Lc, sneezing, and vomiting had revealed the brainstem region that can be specifically stimulated during particular behavior, e.g. LRN neurons in the reflexes triggered from the middle and lower airways (the AR, cough, and ER) or the medullary raphe in AR and emesis. The neurons within the rostral ventrolateral medulla and the rostral mesencephalon seem to contribute solely to forceful expirations while those within the medullary tegmental fields, the rostral dorsolateral pons, the central tegmental field of caudal mesencephalon might be involved in generation of massive inspiratory efforts. We propose that the pre-motoneuronal areas of the caudal and intermediate VRG appear more complex, probably containing additional neuronal populations with inhibitory interneurons or the „behavioral control elements“ that are involved in processing of the studied reflexes.

REFERENCES

1. Korpáš J, Tomori Z. Cough and other respiratory reflexes. New York: S Karger, Basel; 1979.
2. Batsel HL, Lines AJ. Discharge of respiratory neurons in sneezes resulting from ethmoidal nerve stimulation. Exp Neurol 1978; 58(3): 410-24.
3. Jakuš J, Tomori Z, Stránsky A. Activity of bulbar respiratory neurones during cough and other respiratory tract reflexes in cats. Physiol Bohemoslov 1985; 34: 127-36.
4. Shannon R, Baekey DM, Morris KF, Lindsey BG. Ventrolateral medullary respiratory network and a model of cough motor pattern generation. J Appl Physiol 1998; 84(6): 2020-35.
5. Baekey DM, Morris KF, Nuding SC Segers LS, Lindsey BG, Shannon R. Ventrolateral medullary respiratory network participation in the expiration reflex in the cat. J Appl Physiol 2004; 96: 2057-72.
6. Dyachenko YE. Spontaneous and evoked activity of bulbar respiratory and nonrespiratory neurons during the expiration reflex. Neirofiziologija 1990; 22: 670-80.
7. Baekey DM, Morris KF, Nuding SC, Segers LS, Lindsey BG, Shannon R. Medullary raphe neuron activity is altered during fictive cough in the decerebrate cat. J Appl Physiol 2003; 94: 93–100.
8. Jakuš J, Stránsky A, Poliaček I, Baráni H, Bošeľová Ľ. Effects of medullary midline lesions on cough and other airway reflexes in anaesthetized cats. Physiol Res 1998; 47: 203-13.
9. Jakuš J, Stránsky A, Poliaček I, Baráni H, Bošeľová Ľ. Kainic acid lesions to the lateral tegmental field of medulla: effects on cough, expiration and aspiration reflexes in anesthetized cats. Physiol Res 2000; 49: 387-98.
10. Poliaček I, Jakuš J, Stránsky A, Baráni H, Halašová E, Tomori Z. Cough, expiration and aspiration reflexes following kainic acid lesions to the pontine respiratory group in anesthetized cats. Physiol Res 2004; 53: 155-63.
11. Poliaček I, Corrie LW, Wang C, Rose MJ, Bolser DC. Microinjection of DLH into the region of the caudal ventral respiratory column in the cat: evidence for an endogenous cough-suppressant mechanism. J Appl Physiol 2007; 102(3): 1014-21.
12. Bonham AC, Chen CY, Sekizawa SI, Joad JP. Plasticity in the nucleus tractus solitarius and its influence on lung and airway reflexes. J Appl Physiol 2006; 101: 322-27.
13. Shannon R, Baekey DM, Morris KF, Nuding SC, Segers LS, Lindsey BG. Production of reflex cough by brainstem respiratory networks. Pulm Pharmacol Ther 2004; 17(6): 369-76.
14. Bianchi AL, Denavit-Saubie M, Champagnat J. Central control of breathing in Mammals: Neuronal circuitry, membrane properties, and neurotransmitters. Physiol Rev 1995; 75: 1-45.
15. Iscoe S. Control of abdominal muscles. Prog Neurobiol 1998**;** 56: 433-506.
16. Jakuš J, Tomori Z, Stránsky A. Neuronal Determinants of Breathing, Coughing and Related Motor Behaviours. Martin: Wist; 2004.
17. Bolser DC, Poliaček I, Jakuš J, Fuller DD, Davenport PW. Neurogenesis of cough, other airway defensive behaviors and breathing: a holarchical system? Respir Physiol Neurobiol 2006; 152: 255-65.
18. Jakuš J, Halašová E, Poliaček I, Tomori Z, Stránsky A. Brainstem areas involved in the aspiration reflex: c-fos study in anaesthetized cats. Physiol Res 2004; 53: 703-17.

19. Jakuš J, Poliaček I, Halašová E, Muríň P, Knociková J, Tomori Z, Bolser DC. Brainstem Circuitry of Tracheal-bronchial Cough: c-fos Study in Anesthetized Cats. Respir Physiol Neurobiol 2008; 160: 289-300. DOI information: 10. 1016/j.resp.2007.10.014.
20. Poliaček I, Halašová E, Jakuš J, Muríň P, Baráni H, Stránsky A, Bolser DC. Brainstem regions involved in the expiration reflex. A *c-fos* study in anesthetized cats. Brain Res 2007; 1184: 168-77. DOI information: 10.1016/j.brainres.2007.09.064.
21. Wallois F, Gros F, Masmoudi K, Larnicol N. C-Fos-like immunoreactivity in the cat brainstem evoked by sneeze-inducing air puff stimulation of the nasal mucosa. Brain Res 1995; 687: 143-54.
22. Gestreau C, Bianchi Al, Grelot L. Differential brainstem Fos-like immunoreactivity after laryngeal-induced coughing and its reduction by codeine. J Neurosci 1997; 17: 9340-52.
23. Dragunow M, Robertson HA. Localization and induction of c-fos proteine-like immunoreactive material in the nuclei of adult mammalian neurons. Brain Res 1988; 440: 252-60.
24. Morgan JI, Curran T. Stimulus-transcription coupling in the nervous system: involvement of the inducible proto-oncogenes fos and jun. Annu Rev Neurosci 1991; 14: 421-51.
25. Miller AD, Ruggiero D. Emetic reflex arc revealed by expression of the immediate-early gene c-Fos in the cat. J Neurosci 1994; 14: 871-88.
26. Lykkegaard K, Lauritzen B, Tessem L, Weikop P, Svendsen O. Local anaesthetics attenuates spinal nociception and HPA-axis activation during experimental laparotomy in pigs. ResVet Sci 2005; 79: 245–51.
27. Orendáčová J, Maršala M, Šulla I, Kaľka J, Jalč P, Čížová D, Taira Y, Maršala J. Incipient cauda equina syndrome as a model of somatovisceral pain in dogs: Spinal cord structures involved as revealed by the expression of c-fos and NADPH diaphorase activity. Neurosci 2000; 95: 543-57.
28. Berman AL. The brainstem of the cat. A cytoarchitectonic atlas with stereotaxic coordinates. Madison: The University of Wisconsin press; 1968.
29. Kalia M, Mesulam MM. Brain stem projections of sensory and motor components of the vagus complex in cat. II. Laryngeal, tracheobronchial, pulmonary, cardiac, and gastrointestinal branches. J Comp Neurol 1980; 193: 467-508.
30. Petrovický P. Reticular formation and its raphe system I. Cytoarchitectonics with comparative aspects. Prague: Acta Univ Carolinae Med Monographia XLIX; 1980.
31. Dampney RAL, Horiuchi J. Functional organisation of central cardiovascular pathways: studies using c-*fos* gene expression. Prog Neurobiol 2003; 71: 359–84.
32. Dyachenko YE. Neurophysiological study of bulbar projections of different groups of superior laryngeal afferents. Neirofiziologija 1988; 20: 81-90.
33. Jordan D. Central nervous control of the airways. In: Jordan D editor. Central Nervous Control of Autonomic Function. Chur: Harwood Academic Publishers; 1997. p. 63-107.
34. Jordan D. Central nervous pathways and control of the airways. Respir Physiol 2001; 125: 67-81.
35. Kubin L, Alheid GF, Zuperku EJ, McCrimmon DR. Central pathways of pulmonary and lower airway vagal afferents. J Appl Physiol 2006; 101: 618–27.
36. Miller AD. Central mechanisms of vomiting. Dig Dis Sci 1999; 44(8 Suppl): 39S-43S.
37. Onishi T, Mori T, Yanagihara M, Furukawa N, Fukuda H. Similarities of the neuronal circuit for the induction of fictive vomiting between ferrets and dogs. Auton Neurosci 2007; 136(1-2): 20-30.
38. Davies RO, Kubin L, Pack AL. Pulmonary stretch receptor relay neurones of the cat: location and contralateral medullary projections. J Physiol 1987; 383: 571-85.
39. Mutolo D, Bongianni F, Fontana GA, Pantaleo T. The role of excitatory amino acids and substance P in the mediation of the cough reflex within the nucleus tractus solitarii of the rabbit. Brain Res Bull 2007; 74(4): 284-93.
40. Menetrey D, Gannon A, Levine JD, Basbaum AI. Expression of c-fos protein in interneurons and projection neurons of the rat spinal cord in response to noxious somatic, articular, and visceral stimulation. J Comp Neurol 1989; 285: 177-95.
41. Arita H, Kogo N, Koshiya N. Morphological and physiological properties of caudal medullary expiratory neurons of the cat. Brain Res 1987; 401(2): 258-66.
42. Fung ML, Tomori Z, St John WM. Medullary neuronal activities in gasping induced by pharyngeal stimulation and hypoxia. Respir Physiol 1995; 100(3): 195-202.
43. Korpáš J, Jakuš J. The expiration reflex from the vocal folds. Acta Physiol Hung 2000; 87: 201-15.
44. Tanaka Y, Yoshida Y, Hirano M. Expression of Fos-protein activated by tactile stimulation on the laryngeal vestibulum in the cat's lower brain stem. J Laryng Otol 1995; 109: 39-44.
45. Ambalavanar R, Tanaka Y, Selbie WS, Ludlow CL. Neuronal activation in the medulla oblongata during selective elicitation of the laryngeal adductor response. J Neurophysiol 2004; 92: 2920-32.
46. Fukuda H, Koga T. Non-respiratory neurons in the Bötzinger complex exhibiting appropriate firing patterns to generate the emetic act in dogs. Neurosci Res 1992; 14(3): 180-94.
47. Bongianni F, Mutolo D, Fontana GA, Pantaleo T. Discharge patterns of Bötzinger complex neurons during cough in the cat. Am J Physiol 1998; 274 (Regulatory Integrative Comp Physiol 43): R1015–24.
48. Feldman JL, Mitchell GS, Nattie EE. BREATHING: Rhythmicity, Plasticity, Chemosensitivity. Annu. Rev Neurosci 2003; 26: 239–66.
49. Nattie E, Li A. Retrotrapezoid nucleus lesions decrease phrenic activity and CO2 sensitivity in rats. Respir Physiol 1994; 97(1): 63-77.

50. Bodineau L, Frugiere A, Marlot M, Wallois F. Effect of hypoxia on the activity of respiratory and non-respiratory modulated retrotrapezoid neurons of the cat. Auton Neurosci 2000; 86(1-2): 70-7.
51. Larnicol N, Wallois F, Berquin P, Gros F, Rose D. C-fos-like immunoreactivity in the cat's neuraxis following moderate hypoxia or hypercapnia. J Physiol 1994; 88: 81-8.
52. Teppema LJ, Berkenbosh A, Veening JG, Olivier CN. Hypercapnia induces c-fos expression in neurons of retrotrapezoid nucleus in cats. Brain Res 1994; 635: 353-6.
53. St John WM. Neurogenesis, control, and functional significance of gasping. J Appl Physiol 1990; 68: 1305-15.
54. St John WM. Medullary regions for neurogenesis of gasping: noeud vital or noeuds vitals. J Appl Physiol 1996; 81: 1865-77.
55. Fung ML, St John WM, Tomori Z. Reflex recruitment of medullary gasping mechanisms in eupnoea by pharyngeal stimulations in cats. J Physiol Lond 1994; 475: 519-29.
56. Scheibel AB: The brain stem reticular core and sensory function. In Handbook of Physiology. The Nervous System, Sensory Processes. Bethesda: American Physiological Society; 1984. p. 213-56.
57. Billig I, Foris JM, Enquist LW, Card JP, Yates BJ. Definition of neuronal circuitry controlling the activity of phrenic and abdominal motoneurons in the ferret using recombinant strains of pseudorabies virus. J Neurosci 2000; 20(19): 7446-54.
58. Shannon R, Baekey DM, Morris KF, Nuding SC, Segers LS, Lindsey BG. Pontine respiratory group neuron discharge is altered during fictive cough in the decerebrate cat. Respir Physiol Neurobiol 2004; 142: 43–54.
59. Maršala J, Lukáčová N, Čížková D, Kafka J, Katsube N, Kuchárová K, Maršala M. The case for the bulbospinal respiratory nitric oxide synthase-immunoreactive pathway in the dog. Exp Neurol 2002; 177: 115-32.
60. Otake K, Ezure K, Lipski J, Wong She RB. Projections from the commissural subnucleus of the nucleus of the solitary tract: an anterograde tracing study in the cat. J Comp Neurol 1992; 324: 365-78.
61. Smith JC, Morrison DE, Ellenberger HH, Otto MR, Feldman JL. Brainstem projections to the major respiratory neuron populations in the medulla of the cat. J Comp Neurol 1989; 281: 69-96.
62. Bandler R Shipley MT. Columnar organization in the midbrain periaqueductal gray: modules for emotional expression? Trends Neurosci 1994; 17: 379–89.
63. Davis PJ, Zhang SP, Winkworth A, Bandler R. Neural control of vocalization: respiratory and emotional influences. J Voice 1996; 10: 23–38.
64. Guo ZL, Li P, Longhurst JC. Central pathways in the pons and midbrain involved in cardiac sympathoexcitatory reflexes in cats. Neuroscience 2002; 113: 435-47.
65. Chen G, Aston-Jones G. Extensive projections from the midbrain periaqueductal gray to the caudal ventrolateral medulla: a retrograde and anterograde tracing study in the rat. Neuroscience 1996; 71: 443-59.
66. Hudson PM, Lumb BM. Neurons in the midbrain periaqueductal gray send collateral projections to nucleus raphe magnus and the rostral ventrolateral medulla in the rat. Brain Res 1996; 733: 138-41.
67. Holstege G, Kuypers HGJM: Propriobulbar fibre connections to the trigeminal, facial and hypoglossal motor nuclei. I. An anterograde degeneration study in the cat. Brain 1997; 100: 239-42.
68. Roste LS, Dietrichs E, Walberg F. A projection from the the periaqueductal grey to the lateral reticular nucleus in the cat. Anat Embryol (Berlin) 1985; 172: 339-43.
69. Ambalavanar R, Tanaka Y, Damirjian M, Ludlow CL. Laryngeal Afferent Stimulation Enhances Fos Immunoreactivity in Periaqueductal Gray in the Cat. J Comp Neurol 1999; 409: 411–23.

Acknowledgement
We gratefully acknowledge the technical assistance of Eva Frolová, Peter Macháč and Roman Kubizňa.
This study was supported by grants to Prof. Ján Jakuš : No. 1/2274/05 (VEGA) from the Grant Agency for Science of the Slovak Republic and No. 20 - 04 7705 (APVV).

Received: December, 12, 2007
Accepted: April 14, 2008

DETECTION OF HYPERMETHYLATION OF P16 PROMOTER REGION IN GASTROINTESTINAL STROMAL TUMORS BY METHYLATION-SPECIFIC PCR

ZORA LASABOVÁ[1*], PETRA TILANDYOVÁ [2], ANDREA VAŇOCHOVÁ [1], TATIANA BURJANIVOVÁ [2], GABRIEL MINÁRIK [4], PETER SZÉPE [3], KAROL KAJO [3], KATARÍNA MACHÁLEKOVÁ[3], LUKÁŠ PLANK [3]

Laboratory of Molecular Biology of Department of Molecular Biology[1] and Department of Pathological Anatomy [2], and Department of Pathological Anatomy [3], Jessenius Faculty of Medicine of Comenius University and Faculty Hospital, Martin, Geneton s.r.o.[4], Bratislava, Slovak Republic

Abstract

Gastrointestinal stromal tumors (GIST) are the most common mesenchymal tumors of the gastrointestinal tract generally expressing CD117 (KIT) and harboring activating mutation in protooncogenes either c-kit or PDGFRa. Recently, it was reported, that loss of the p16 protein detected by immunohistochemistry in tissue microarrays was associated with high risk tumors in patients with GIST. We developed nested methylation specific PCR for detection of hypermethylation of the promoter region of the p16 confirmed by bisulfite sequencing and determined the methylation status of the promoter region of the p16 gene and compared it with the pathological findings considering the prognostic potential of the hypermethylation in the promoter region of p16 gene. After examination of twelve patients with different histopathological characterization we showed that hypermethylation of the p16 promoter region is a common event in GIST and independent of clinical stage as well as of risk of malignant behavior evaluated by histopathological criteria.

Key words: promoter hypermethylation, gastrointestinal stromal tumors , p16

INTRODUCTION

Gastrointestinal stromal tumors (GIST) are the most common mesenchymal tumors of the gastrointestinal tract generally expressing CD117 (KIT) and harboring activating mutation in protooncogenes either in c-kit or PDGFRa. The mutations within these genes are mutually exclusive and were observed in more than 80% of sporadic GIST. These mutations are somatic and present only in tumor tissue in contrast to similar constitutional mutations in familial GIST which are present in all cells of the body. The tumors are highly resistant to conventional chemotherapy and prediction of prognosis of primary tumor is a topic of intensive research (1-3). The most reliable and generally clinically accepted prognostic factors are the size of the primary tumor and the mitotic activity. Small tumors (less than 5 cm) with low mitotic frequency have usually a benign clinical outcome; however, small subsets of mitotically active tumor cells have metastazing properties (1, 4). According to these criteria, the patients with GIST can be classified as patients with tumours of high risk, intermediate and low or very low risk of malignancy (4). Additional prognostic factors were tested in different clinical studies like telomerase activity, aneuploidy in DNA flow cytometry, KIT mutations, and presence of tumor necrosis or hypermethylation of promoter regions of tumor suppressor genes (3).

Epigenetic mechanisms such as DNA methylation play an important role in human carcinogenesis. The methylation produces modifications of DNA that may affect gene expression in a heritable manner without alteration of the nucleotide sequences. Methylation of

Address for correspondence:
RNDr. Zora Lasabová PhD, Department of Molecular Biology, Jessenius Faculty of Medicine of Comenius University in Martin, Kalinčiaka 2, 03861 Vrútky, Slovakia. Phone: 00421-43-4286517, e-mail:

DNA occurs on cytosine residues on the CpG dinucleotides, which are not randomly distributed throughout the genome; rather they are frequently clustered into CpG islands found in the promoter regions of the genes. CpG islands are generally unmetylated in normal adult tissue, but most cancer tissues demonstrate promoter hypermethylation in certain tumor suppressor genes and the methylation of these CpG sites can lead to repression of the gene expression (5-6). Reversal of hypermethylation and up-regulation of the tumor suppressor genes has therefore become a new therapeutic target in cancer treatment (7). Genetic changes in gene coding for cell cycle regulators have been related to proliferation and progression of cancer cell. The p16 tumor suppressor gene mapped to 9p11 belongs to such critical genes and inhibits cell cycling by arresting cells in G_1-S phase of the cell cycle (8). Recently it was reported, that loss of the p16 protein detected by immunohistochemistry in tissue microarrays was associated with high risk tumors in patients with GIST (9). The methylation-specific PCR (MSP) is a sensitive and specific method for detection of methylation of CpG sites within a CpG islands. MSP consists of bisulfite modification followed by amplification with methylation specific primers (10). Bisulfite modification creates the sequence differences between the methylated and unmethylated DNA and different primers can be designed to distinguish methylated from unmethylated DNA. In a recent study, we developed nested methylation specific PCR for detection of hypermethylation of the promoter region of the p16 confirmed by bisulfite sequencing and determined the methylation status of the promoter region of the p16 gene and compared it with the pathological findings considering the prognostic potential of the hypermethylation in the promoter region of p16 gene.

MATERIAL AND METHODS

Patients and human tissue samples

Paraffin-embedded tissue sections (sectioned at the thickness of 6 μm) were obtained from biopsy specimens of twelve patients with histologically confirmed GIST that were presented to the department of pathology. Characterization of tumor samples, including tumor size, histology, mitotic rate, CD117 and, CD34 expression was carried out by experienced pathologist examining the tissue sections.

DNA Preparation

Genomic DNA was isolated from paraffin sections after paraffin removing in xylen and rehydratation through a series of descending concentrations of alcohol (96 %, 80 %, and 70 %) for 15 min each of them. DNA was isolated using the Wizard® Genomic DNA purification kit (Promega, USA) according to the manufacturer protocol. Briefly, 50 μl of Nuclei Lysis Solution was added to the tube containing the resuspended cells from the deparaffined sections of the patients with GIST and the samples were incubated at 56°C overnight. Afterward, the proteins were precipitated by adding of 50 μl Protein Precipitation Solution. After centrifugation, the supernatant was transferred to a clean microcentrifuge tube containing 150 μl of isopropanol, DNA was precipitated, centrifuged and after washing in 70% ethanol resolved in TE buffer. The concentration of DNA was determined in a spectrophotometer at 260 nm.

Bisulfite Treatment

Sodium bisulfite conversion of unmethylated cytosine residues to uracil in samples of genomic DNA obtained from patient tissue samples with gastrointestinal stromal tumor (GIST) was performed by using the CpGenome™ DNA Modification Kit (Chemicon, USA) according to the protocol of the manufacturer. Briefly, 5-8 μg of genomic DNA resolved in 100 μl of H_2O were denaturated with 7.0 μl of 3 M NaOH and incubated overnight. DNA was

then bound to a 5 μl micro-particulate carrier in the presence of another salt 750 μl of Reagent II responsible for desulfonation. Then after, the modified DNA was desalted by repeated centrifugation and resuspension in 70% ethanol. The DNA was finally eluted from the carrier by heating in 25 μl TE buffer, pipetted in 5 μl aliquots and stored at -20°C.

Methylation Specific Polymerase Chain Reaction

PCR reaction was performed with 2.0 μl of bisulfite modified DNA template in 25 μl of reaction mixture containing 2.5 mmol/L $MgCl_2$, 10 pmol/L of each forward and reverse primer, 0.5 mmol/L of each of the four dNTPs, 2.5 mmol/L of 10x PCR Buffer (ABgene®, United Kingdom). Negative control samples without DNA were included for each set of PCR. There were used primer pairs for the detection of methylated DNA (10) in p16 target sequence p16-M2 forward 5'-TTATTAGAGGGTGGGGCGGATCGC and p16M2 reverse 5'-CCACCTAAATCGACCTCCGACCG (MSP primers), and for the detection of unmethylated target sequence p16-U forward 5'-TTATTAGAGGGTGGGGTGGATTGT and p16-U reverse 5'-CAACCCCAAACCACAACCATAA (USP primers).

PCR reaction was performed in duplicate and was subjected to hot start at 95°C for 8 min followed by 35 cycles of denaturation at 95°C for 30 seconds, annealing temperature used for MSP primers was 65°C for 30 seconds and for USP primers was 60°C for 30 seconds followed by extension at 72 °C for 30 seconds, and the final step of 4 minutes at 72°C.

Twelve μl of each PCR reaction were loaded onto 1.75% agarose gel, stained with ethidium bromide and visualized under UV illumination. We used 50 bp ladder. The PCR product for MSP primers (p16-M2) had extent 234 bp and for USP primers (p16-U) had extent 151 bp.

We performed a second round PCR reaction using 1 μl of the PCR product obtained in the first round PCR by application of the same primers and the same PCR conditions as described above. The reamplification products were analyzed on an ethidium bromide stained agarose gel and subsequently sequenced.

Sequencing of the PCR products specific for methylated and unmethylated DNA (Bisulfite sequencing)

To validate the methylation-specific PCR and quantify the extent of the methylation at the CpG sites, we performed a DNA sequencing of reamplified PCR products. The PCR products were purified by NucleoSpinExtract II kit (Machery and Nagel, Germany) and cycle sequenced by BigDye Terminator v1.1 Cycle Sequencing Kit (ABI, USA) using primers p16-M2 forward and reverse at 59 °C, and primers p16-U forward and reverse at 59°C for methylated and unmethylated template, respectivelly. The sequences were analyzed in ABI PRISM 3130 genetic analyzer, by Chromas software and compared to GenBank sequence NM058197.

RESULTS

Using the methylation specific PCR, we examined the methylation status of promoter region of p16 gene in paraffin sections of twelve patients with gastrointestinal stromal tumors (GIST). The patients were examined by pathologist according to the criteria of bioptical diagnosis and the results of histopathological findings and immunohistochemistry are summarized in the table 1. The twelve patients were of different histopathological characteristics concerning the risk of malignant behavior as high risk (6 patients), intermediate risk (2 patients) and low or very low risk (4 patients). The localization of the tumor was mostly in stomach (8 patients), small intestine (2 patients), rectum (one patient) and one e-GIST. The DNA from paraffin-embedded tissue of these patients was isolated and subjected to bisulfite modification and PCR. Using primers specific for methylated DNA, p16Mforward (p16MF) and p16Mreverse (p16MR), we were able to detect PCR products of expected size in three as high risk evaluated patient samples in ethidium bromide stained agarose gel.

(Fig.1 A). The CpGenome Universal Methylated DNA (Chemicon, USA), the positive control for completely methylated DNA, showed methylation specific product with strong signal (Fig.1A, lane 4). The bisulfite modified DNA from these three patients was subjected to a PCR reaction with primers specific for unmethylated DNA p16UR and p16UF. We obtained very weak visible PCR products specific for unmethylated DNA (Fig 1B). The specificity of this reaction was controlled by negativity of the CpGenome Universal Methylated DNA (Fig.1B, lane 4), which has methylated CpG sites within the whole genome, including the target sequence between the primers p16UF and p16UR. The products of both type of the PCR reaction were weak visible and the amount of the products was insufficient for performing a validating sequencing analysis. For that reason, we reamplified the PCR products from patient 1 (Fig.1A, lane 1) and completely methylated control sample (Fig. 1A, lane 4) with primers p16MF and p16MR and PCR product from patient 3 (Fig. 1B, lane 1) with primers p16UF and p16UR, respectively and the resulting PCR products were subjected to subsequent sequencing with primers p16MF, p16MR and p16UF, p16UR, specific for methylated or unmethylated template, respectively. After bisulfite sequencing (Fig. 2A) and comparison of the obtained DNA sequences with the GenBank sequence NM94157 (a part of the p16 gene) between nucleotides 136 and 241, we detected 12 different CpG sites, which remained unmodified in the DNA sequence gained with p16MF primer and showed C at each CpG site (Fig. 2B), what is evidence of methylation of these particular cytosines. The sequence of the PCR product with p16UF primers was modified at C of CpG sites and showed the change from C to T, what is the evidence for cytosines without methylation.

After providing evidence, that our PCR with primers p16MF and p16MR, and primers p16UF and p16UR, are specific for detection of methylated and unmethylated DNA after reamplification, we subjected the DNA isolated from paraffine section of patients with GIST showed in Table1 to bisulfite modification and subsequent MSP PCR. We again obtained PCR products with primers specific for umethylated DNA, which is explained by occurrence of non tumor tissue (data not shown). Using methylation specific primers p16MF and p16MR, we were able to detect reamplified methylation specific PCR products of expected

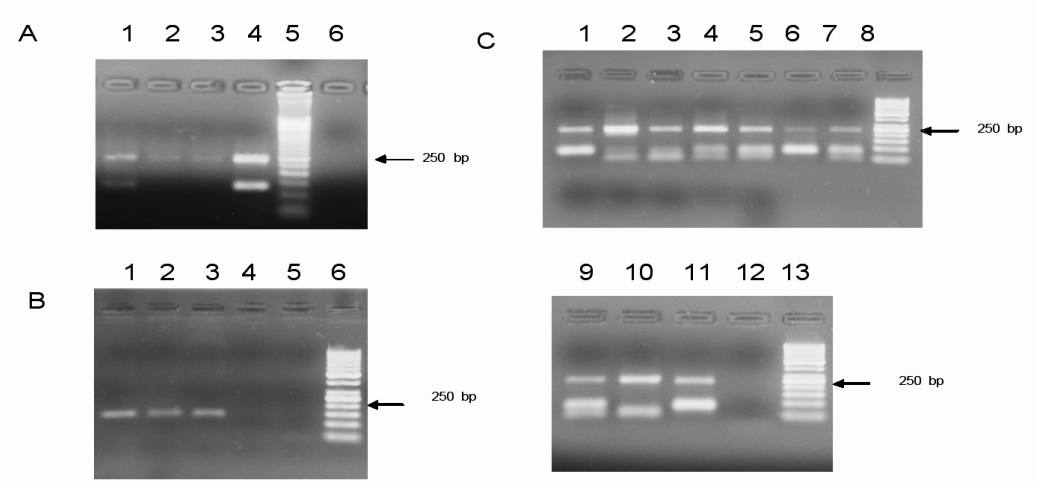

Figure 1. A Results of methylation-specific PCR using primers p16MF and p16MR detecting methylated DNA and yielding a 234 bp PCR product. *Lanes 1, 2, 3 patients with high risk GIST (patients 1, 2 and 3), lane 4 is the CpGenome Universal Methylated DNA, lane 5 50 bp ladder, line 6 PCR negative control.* B Amplification of bisulfite modified DNA using p16UF and p16UR primers detecting unmethylated DNA and yielding 151 bp PCR product. *In lanes 1, 2, 3 are samples from patiens 1, 2, 3, lane 4 is the CpGenome Universal Methylated DNA, lane 5 is PCR negative control, lane 6 is 50 bp ladder.* C. Reamplification of the first round PCR products from the bisulfite modified patiens DNA with the primers p16M and p16MF from patiens with GIST (lanes 1-10), completely methylated DNA (lane 11) and negative control of PCR. *Lane 13 is 50 bp ladder.*

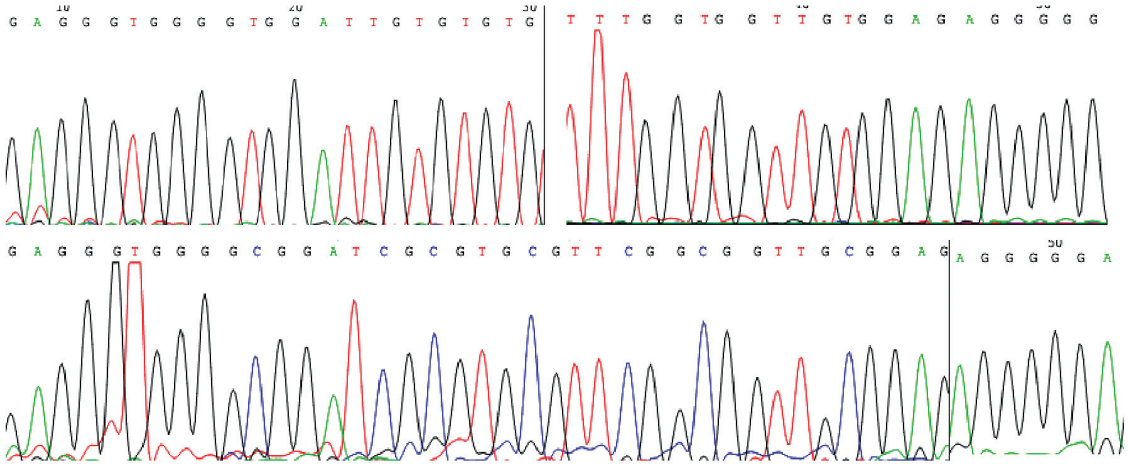

NM94157	5'	C	A	G	A	G	G	G	T	G	G	G	G	**C**	**G**	G	A	**C**	**C**	**G**	**C**	**G**	T	G	**C**	**G**	C	T	**C**	**G**	G
PCR methyl														C					C		C				C				C		
PCR unmethyl														T					T		T				T				T		
		C	**G**	G	C	T	G	**C**	**G**	G	A	G	A	G	G	G	G	G	A	G	A	G	C	A	G	G	C	A	G	**C**	G
		C						C																					C		
		T						T																					T		
		G	G	**C**	**G**	G	**C**	**G**	G	G	G	A	G	C	A	G	C	A	T	G	G	A	G	C	**C**	**G**	G	**C**	**G**	G	**C**
				C			C																		C			C			C
				T			T																		T			T			T

Fig.2 A A part of the DNA sequence from reamplified by MSP with primers p16UF and p16UFR (upper) and p16MF and p16MR (lower sequence) specific for unmethylated and methylated DNA, respectively B Comparison of the sequences with the NM94157 GeneBank sequences (see text).

size in each sample evalutated (Fig. 1C), independently of clinical stage and histopathological evaluation, but we were not able to examine normal gastric tissue to compare the occurrence of the hypermethylation of the p16 with this type of clinical samples. Our results showed, that we developed a methylation specific PCR for detection of hypermethylation within the promoter region of the p16 gene and were able to quantify the extent of methylation by bisulfite sequencing. The sequencing showed, that in the patients control sample, and in the CpG Genome Hypermethylated control DNA all 12 CpG sites from 12 were methylated (Fig.2). After examination of twelve patients with different histopathological characterization we showed, that after reamplification of methylation specific PCR we found methylated DNA in each sample examined.

Table1. Pathological characteristics of patients with GIST.

Nr.	Risk of malignant behaviour	Localization	Tumor subtype	Necrosis	metastases	Expression of CD117and CD34
1	High risk	stomach	Spindle cell type	+	retroperiteneal	CD117+/CD34-
2	High risk	e-GIST	Spindle cell type	+	stomach	CD117+/CD34+
3	High risk	rectum	Mixed cell type	+	unknown	CD117+ <10%, CD34-
4	Low risk	stomach	spindle	no	unknown	CD117+/CD34+
5	Low risk	stomach	Epitheloid cell type	no	unknown	CD117+/CD34+
6	Intermediate risk	small intestine	Spindle cell type	no	unknown	CD117+/CD34- (CD34+ in <0%)
7	High risk	2 tumors stomach + mesentery	Mixed cell type	+	mesenterial	CD117-/CD34-
8	Low risk	stomach	Spindle cell type	no	unknown	CD117+/CD34+
9	High risk	mesentery (e-GIST ?)	Spindle cell type	no	?	CD117+/CD34+
10	Very low risk	stomach	Epitheloid cell type	no	unknown	CD117+/CD34+
11	Intermediate risk	stomach	Spindle cell type	no	unknown	CD117+/CD34+
12	High risk	small intestine	Spindle cell type	+	unkown	CD117+/ CD34+<50%,

DISCUSSION

The GIST represents a cancer showing heterogenous clinical symptomatology and a broad spectrum of behavior ranging from benign or very low malignant to highly malignant and aggressive tumours (1). The bioptical diagnosis has very good tools to discriminate between high and low risk patients (1-3), but there are several indications that molecular alterations may predict the clinical outcome. Recently, the loss of p16 protein detected by immunohistochemistry was reported in tissues from patients with GIST and correlated to worse prognosis (9). The epigenetic changes are a topic of intensive research in cancer genetics and are considered to be one of the important mechanisms of gene expression inactivation (5). We studied the hypermethylation of the promoter region of p16gene considering with the question, if this event could be predictive for disease behavior.

Here we report about development and implementation of methylation-specific PCR and study of the promoter hypermethylation of p16 in paraffin sections of patients with GITS, which was validated by bisulfite sequencing. By two round MSP, we demonstrated the hypermethylation of p16 promoter in all tested patient samples, regardless of the clinical stages and histopathological criteria. Recently, only one publication analyzed the hypermethylation of p16 in GIST (11) with detection p16 hypermethylation in 45% tested clinical samples independently of clinical stage and histopathological criteria, but this frequency is much lower as the frequency in our study. The reason could be that the two round PCR assay, which is a very sensitive method, enables us to detect the lowest amounts of methylated DNA. Normal gastric tissue from healthy persons is considered to be negative for methylation in p16 gene, but a very low level of hypermethylation is possible in normally

appearing tissue from cancer patients (12), so very important step in such study is to compare the DNA isolated from tissues of patients with other non-neoplastic disorders and from normally appearing tissues. For this study, we were not able to study normal gastric tissue and to develop a threshold for methylation level occurred within a normal tissue. We consider involving this tissue comparison in the future and so develop a method, which can better distinguish between cancer and normal gastric tissue. We also have shown that our PCR with primers specific for unmethylated DNA was specific for unmethylated DNA, including the negative PCR result of the CpGenome Universal Methylated DNA control sample. The high levels of unmethylated DNA could be a result of the high amounts of normal tissue within the paraffin section. We can conclude that the hypermethylation of p16 promoter region is a common event in cancer tissue of patients with GITS, which is present at different stages of the clinical course of the disease and is present already at early stage of the tumor development. It is necessary to examine the threshold for methylation comparing cancer and normal gastric tissue and to quantify the amounts of methylated DNA. Other important problem to solve is the isolation of cancer tissue by microdissection and to examine such isolated DNA on methylation compared with normal tissue. The epigenetic mechanism of gene silencing is involved in progression of tumors and determination of hypermethylation of the promoter regions of certain cancer critical genes is a very promising approach in searching for new biomarkers of cancer development and progression. In contrast to loss of heterozygosity, the hypermethylation is a reversible process and a possible target for therapy, what makes it an candidate for monitoring of diseases.

REFERENCES

1. Plank L. Bioptická diagnostika gastrointestinálnych stromálnych nádorov. Onkológia 2007; 2:85-92
2. Daum O, Vaneček T, Šíma R, Michal M. Gastrointestinální stromální tumor: současný pohled. Gastrointestinal stromal tumor: Update. Klinická onkologie 2006; 19: 203-211
3. Rubin PB, Heinrich MC, Corless CL. Gastrointestinal Stromal Tumour. Lancet 2007: 369: 1731-1741
4. Miettinen M, Lasota J. Gastrointestinal Stromal Tumors. Review of Morphology, Molecular Pathology, Prognosis, and Differential Diagnosis. Arch Pathol Lab Med 2006; 130: 1466-1478
5. Lofton-Day C, Lesche R. DNA Methylation Markers in Patients with Gastrointestinal Cancer. Digest Dis 2003; 21:299-308
6. Jones PA, Baylin SB. The Epigenomics of Cancer. Cell 2007; 128: 683-692
7. Gilbert J, Gore SD, Herman JG, Carducci MA. The clinical application of targeting Cancer through Histone Acetylation and Hypomethylation. Clin Cancer Res 2004; 10:4589-4596
8. Oue N, Motoshita J, Yokozaki H et al. Distinct promoter hypermethylation of p16INK4a, CDH1 and RAR-ß in intestinal diffuse-adherent and diffuse-scattered type gastric carcinomas. J Pathol 2002; 198: 55-59
9. Schneider-Stock R, Boltze C, Lasota J, Peters B, Corless CL, Ruemmele P, Terracciano L, Pross M, Isabato L, Di Vizio D, Iesalnieks I, Dirnhofer S, Hartmann A, Heinrich M, Miettinen M, Roessner A, Tornillo L. Loss of p16 Protein Defines High-Risk Patients with Gastrointestinal Stromal Tumors: A Tissue Microarray Study. Clin Cancer Res 2005; 11: 638-645
10. Herman JG, Graff JR, Myohanen S, Nelkin BD, Baylin SB. Methylation-specific PCR: A novel PCR assay for methylation status of CpG islands. Proc. Natl Acad Sci 1996; 93: 9821-9826
11. House MG, Guo M, Efron DT, Lillemoe KD, Cameron J, Syphard JE, Hooker CM, Abraham SC, Montgomery E, Herman JG, Brock MV. Tumor Suppressor Gene Hypermethylation as a Predictor of Gastric Stromal Tumor Behavior. J Gastrointestinal Sur 2003; 7: 1004-10014
12. Wang J, Sasco AJ, Fu C, Xue H, Guo G, Hua Z, Zhou Q, Jiang Q, Xu B. Aberrant DNA methylation of P16, MGMZand hMLH1 genes in combination with MTHFR C677T genetic polymorphism in esophageal squamous cell carcinoma. Cancer Epidemiol Biomarkers Prev 2008; 17:118-25

Supported by VEGA grant 1/3373/06 and The educational grant of Novartis Slovakia.
Received: March 18, 2008
Accepted: April 25, 2008

THE ROLE OF BRACHYTHERAPY IN THE TREATMENT OF RELAPSED HIGH GRADE GLIOMAS

[1]EVA HAJTMANOVÁ, [1]ĽUBOŠ ZÁMEČNÍK, [2]JÚLIUS DERIGGO, [3]ANDREJ HAJTMAN
[1]Oncologic Centre, Martin Faculty Hospital, Martin, Slovakia
[2]Department of Neurosurgery, Martin Faculty Hospital, Martin, Slovakia
[3]Clinic of ENT & Head and Neck Surgery of the Jessenius Faculty of Medicine and Martin Faculty Hospital, Martin, Slovakia

Abstract

Primary tumours of the brain represent about 1.5% of all cancers. Patients presenting with malignant glioma will undergo local excision and/or external radiation therapy. Despite this therapy, nearly all tumours will recur. Furthermore, we have been shown that 90% of recurrences occur within 2 cm of the initial tumour. This is mainly due to the poor radiosensitivity of gliomas, and to the fragility of normal brain tissue. Brachytherapy, with its rapid dose fall-off, which offers the opportunity of sparing normal brain tissue, may consequetly constitute an interesting option.

Key words: brachytherapy, interstitial implants, recurrence.

INTRODUCTION

Brachytherapy (sometimes referred to as Curietherapy or endocurie therapy) is a term used to describe short distance treatment of canacer with radiation from small, encapsulated radionuclide sources. This type of treatment is given by placing the sources directly into or near the volume to be treated. The dose then delivered continuostly either over a short period of time - temoporary implants (1). Most common brachytherapy sources emit photons.

Interstitial type of brachytherapy is a treatment where the sources are implanted within the tumour volume.

Interstitial treatment may be temporary or permanent. The temporary implants are carried out using either manual or remote afterloading procedures. The applicator is placed first into the target position and the radioactive sources are loaded later, either by hand (manual afterloading) or by a machine (automatic remote afterloading). Dose is delivered over a short period of time and the sources are removed after the prescribed dose has been reached.

The physical advantage of the brachytherapy treatments compared to external beam radiotherapy is the improved localized delivery of dose to the target volume of interest. The disadvantage is that brachytherapy can only be used in cases where the tumour is well localized and is relatively small.

From a radiobiological point-of-view brachytherapy dose delivery could result in complex dose-rate effects that may also influence the therapeutic outcome. The continuous delivery of dose will influence the repair of sub-lethal and potencially lethal damage, cell proliferation and other cell kinetics, all of which could modify the radiation response of tumour and normal tissues.

Temporary implants of high-activity sources have also been applied occasionally in patients with recurrent brain tumours. High-dose-rate (HDR) remote afterloading units use specially designed Iridium -192 sources with typical activities of 370 GBq (10 Ci), mean energy 360 keV and half-life 74.2 days emits gamma-rays with an average energy of 0.37 MeV as well as 0.67 MeV beta particles (2).

Address for correspondence:
MUDr. Eva Hajtmanová, Onkologické centrum, Martinská fakultná nemocnica, Kollárova 2, 036 59 Martin, Slovak Republik

High-grade gliomas are tumours of neuroepithelial tissue. Anaplastic astrocytoma (AA) corresponds to WHO grade III and glioblastoma mutiforme (GBM) corresponds to WHO grade IV AA is diffusely infiltrating astrocytoma with focal or dispersed anaplasia, and a marked proliferative potential. AA arise from low-grade astrocytomas, but are also diagnosed at first biopsy, without indication of a less malignant precursor lesion. They have an intrinsic tendency for malignant progression to glioblastoma. GBM is the most malignant astrocytic tumour, composed of poorly differentiated neoplastic astrocytes. Glioblastomas may develop from diffuse astrocytomas WHO grade II or anaplastic astrocytomas – secondary glioblastoma, but more frequently , they manifest after a short clinical history de novo, without evidence of a less malignant precursor lesion – primary glioblastoma (3).

The median survival of the patients with diagnosis AA or GMB is after the surgical treatment 3 – 5 months. Postoperated conventional external radiation therapy prolongs the life of patients with glioblastoma multiforme for 9 – 12 months and with anaplastic astrocytoma for 36 months.

Increasing of primary dose radiation ERT from 45 to 60 Gy prolongs the life of patients with malignant gliomas. Increasing TD from 60 to 70 Gy does not prolong ordinary life (4). One of the reason can be also significant increasing risk of radionecrosis origin. This radionecrosis arises to 18 % after the application of TD 65 Gy. Conventional ERT with dose to 60 Gy causes high danger of local recidive (3,4,5,6).

The median patient feeling with recurrent AA after interstitial type of brachytherapy is from 29 to 50 weeks and 42 weeks at patients with recurrence of GMB (1,6,7,8,9).

From the standpoint of cured strategy is important characteristical localization of gliomas recurrence in the place of native centre. 90 % of cases showed tumour recurrence within a 2 cm margin of the primary site (1,5,7,10).

The conformity is an actual trend of radiosurgery. It is a shape adaptation to irradiated size of irregular shape tumour's centre – aim size. Escalation of dose radiation in aim size with technique of conform radiotherapy increases the local control of sickness and contemporary importantly decreases actual toxicity in the tissue (11,12).

Brachytherapy is almost perfect conformal radioterapy what is the main treatment of recurrent tumour in already radiated place. The minimal loads radiation of tissue in the surrounding tumour has mostly at the brain tumour treatment a marked influence for a life quality of the treated patients.

Only a limited number of tumours are eligible for brachytherapy because of the poor tolerance of normal brain to irradiation. IBRT is at malignant gliomas indicated as boost with conventional ERT or as individual paliative treatment the recurrent HG gliomas and single brain metastases (5,8,13,14,15).

PATIENTS AND METHODS

At the Martin Faculty Hospital in 2004 – 2006 treated by radiation were 15 patients with recurrent HG gliomas. In the ensemble there were 11 males and 4 females. Mean age of males was 43 zears and of females 53 years. The malignant tumour was located in 8 cases mostly at the frontal part, in 5 cases at temporal and in 2 cases at parietal part, from those in 11 cases on the left and in 4 cases on the right brain hemisphere.

It was used for the treatment the high dose rate (HDR) afterloading system – MicroSelectron firm Nucletron, with the source of radiation 192 Ir and planning system Plato – version BPS 13.7. Since 2006 has been used Brain-Lab navigated system with the possibility of fusion CT and MR image fusion for the preplanning and the following navigated application brachytherapy catheters.

The diagnosis of the malignant brain tumour was in all patients veryfied by histological examination. In 8 patients it was confirmed GBM and in 7 AA, from that in 3 grade IV. And in 4 patients grade III. All the patients after the diagnosis of malignant tumours were sub-

jected to primary surgeon treatment with the following external radioterapy for a tumour part on average TD 60,0 Gy (50 Gy – 66 Gy).

The recurrent tumour was diagnosted on average 14 months since the primary treatment (3-41 months).

IBRT was indicated a realized in a team work of neuro-oncologist, neurosurgeon and the radiation oncologist.

Patient selection criteria for brain brachytherapy include patient Karnofsky performance status (KPS) score of at least 60 and ability to give informed consent. Tumours must be unifocal, well-circumscribed, supratentorial, and less than 5 to 6 cm in diameter. Large, diffuse tumours and tumours with corpus callosum involvement or subependymal spread are excluded because of their propensity for dissemination, and those involving the cerebellum, brain stem or basal ganglia are excluded on the basis of poor biologic reserve in the event of radiation necrosis (1,4).

Target volume definition

Intersticial BRT needs accurate definition of the seperate aim sizes according to the international recommendations ICRU Report 50, 58 and 62 (16,17,18). The extent of the tumour size was determined by the diagnostic depicted methods – CT, MR examination.

Malignant gliomas are usually enhancing tumours on CT and MRI with mixed signal characteristics of high and low signal intensity regions (Fig.1).

The tumour tissue high grade (HG) gliomas is on CT characterised with mixed signal of high and low density (19, 20). GBM is depicted as the hypodense zone as a rule with masseefect. After of contrast medicine a hypodense ring care be observed in more than 90 % of the patients, so called ring sign. Postcontrast enhancing is signpost of intenzity neoangiogenesis of a tumour tissue and the level of its proliferated activity. Hypodense perifocal zone is caused by necrosis and peritumoural hypodense part creates edema (21, 22). It is an area of the low density in which in uncurable pacients were on post mortem histology veryfied tumour cells. In spite of that is the determination of the borders of tumour in CT image fusion loaded by subjective mistake (7, 13). For MR image fusion is characteristic T1 signal

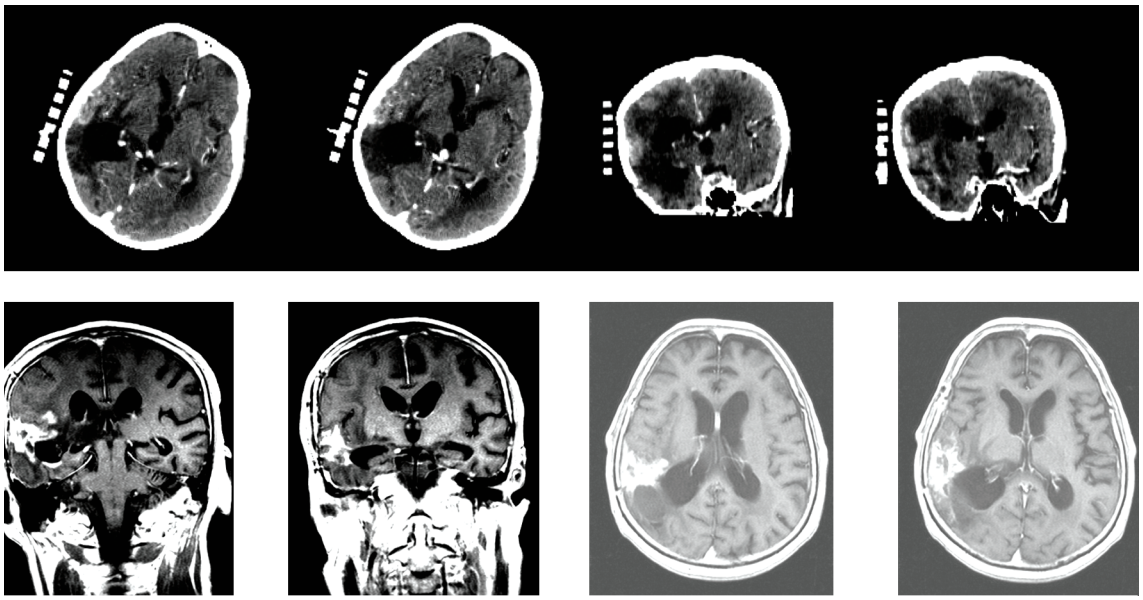

Fig. 1 Localization on CT and MRI with contrast before implantation.

which corresponded with ring sign on CT. On T2 image fusion correspond to peritumoral, hyperintense area with ring – enhancing promontories of tissue, infiltered of tumour's cells together with edema (7, 13, 21, 22).

More complicated was the determination of the target volume at anaplastic astrocytomas, where in the CT image fusion mostly is absented enhancement – the emphasizing after taking of contrast medicine. Tumour tissue is mostly izodense with surrounding brain tissue. For the detemination of the target volume it is necessary to base on CT and MR. On MR examination for the maximum accentuation of details is taken i.v. contrast cure based on Gadolinium. MR image fusion in contrast to CT in not influenced by the close bone structures, mostly in temporal area and fossa posterior.

Generally, if the malignity is higher, then the mass effect is bigger. The differentiatis live tumour tissue from the necrotic one, we use MR spectroscopic and sometimes MR angiographic examination (3,23,19,21,24,25). This methodology enables morphological information with functional information, as the case may be metabolic to make the most accurate of bordered target volume – contouring (26).

Gross tumour volume (GTV) was defined as an area of contrast accent on CT or the area T1 on MR image fusion. Clininal target volume (CTV) presented the area of contrast accent at CT image fusion with hypodense perifocal zone or the area of prolonged T2 weighted signal on MR image fusion with adding of 2-3 cm margin. Planning target volume (PTV) was in brachytherapy the same as CTV, what is another advantage of this therapeutic method (7,18).

Technique with using plexi template

The simulation of irradiated size was realized in irradiated patient position with fixed head by Orfit mask. Orfit termoplastic foil fixed at the same time plexi-template with drilled openings. 2 centimetres in thickness of used plexiglass enabled to keep the direction and constant placement – geometry of implanted catheters. CT examination was made in 3 mm layers which corresponded with the numbers of openings on plexi-template. Contouring of the target volume – CTV/PTV on some CT scans (27) was the result of neuro-oncologist, neurosurgeon and the radiation oncologist. Planning system helped in imaging of target volume the „pre-planning," virtual reconstruction of catheters in different areas with their place and the most accurate lenght of each catheter in tumour tissue, according to the rules by Paris dosimetric system (Fig.2).

Operator, according to the place of target volume and anatomic rates in skull cavity has virtualy corrected a theoretical planned scheme of implantation with operated technique. The nylon catheters neurosurgeon implanted into the brain tissue according to the pre-planning data with the help of plexi-template through the pre-drilling openings in skull bore hole and he fixed them with special plastic collar into the skin.

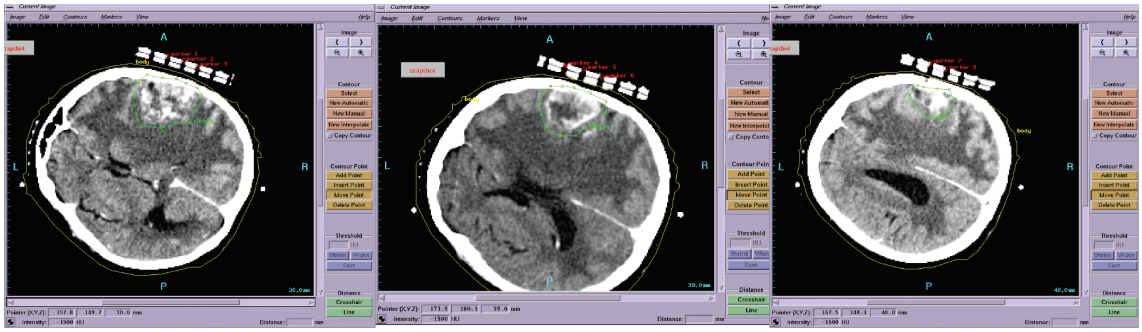

Fig. 2 Virtual pre-planning

Technique with using Brain-Lab navigated system

The simulation of irradiated size was realized in examined position on the back. There was no handmade preparation of Orfit mask and plexi-template. CT examination and surgery were done without any fixed equipment.BrainLab navigated system helped us to use for contouring – an accurate contouring of tumour tissue and for the following pre-planning, CT/MR image fusion of tumour tissue. A virtual place of catheters on CT/MR image fusion was safer because of higher differentiate ability of both imaged examinations in the risk structured CNS areas. More accurate was navigated application catheter for the neosurgeon.

Immidiately after the catheter implantation topographic CT examination followed. It was based on real 3D reconstruction of implantation and planning of dose distribution (Fig.3). Before the planning it was determined in addition to the target volume active (dwell) positions through transport of irid source of radiation. Although geometry of catheters was determined by Paris system, spreading of dose was normalized to CTV/PTV, what, together with geometrical optimalization, caused the increasing of conformity index and higher radiation dose in surrounded healthy tissues. A dose distribution was evaluated with dose – volume histogram (28,29).

All planned TD 30 – 50 Gy took 4 or 5 days. Daily two fractions were applicated in dose 5.0 – 7.0 Gy on fraction, the interval between the applications was minimum 6 hours. During the radiation treatment patients were hospitalized at the neurosurgeon clinic, where in case of complications urgent treatment was provided. During the application BRT patients got corticosteroids, antibiotics and anticonvulsants.

After the application of cure base catheters were removed from the brain tissue. Patients were controlled during 2-months intervals according to recommendation SOMA/LENT scored system (24). To identify a healthy brain tissue from postradiation necrosis, recurrence, persistence of tumour tissue, we started practising MR spektroscopic examination (14,25, 30,31). Because of complicated and long evaluation of examinated area by MR spectroscopy, since 2006 we used hybrid CT/PET scans with using 18-fluoro-deoxyglucose (FDG). From primary brain tumours FDG is increasing mostly in HG gliomas. The advantage of this imaging method is the ability to distinguish the postradiation changes of brain tissue from recurrent tumour. The CT/PET scans help to join the morphological information with functioned information (32,33,34).

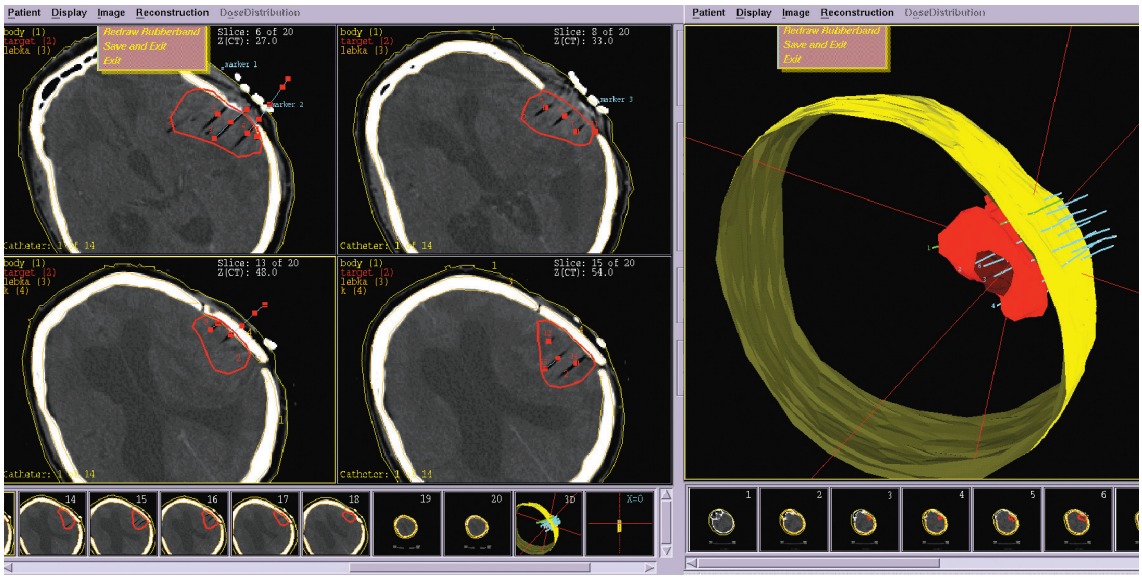

Fig. 3 Treatment planning – CT reconstruction

RESULTS

Results of the treatment were evaluated in only 14 patients.We lost the contact with one patient. In 6 patients (43 %) survival rate was half of a year, in 4 patients (29 %) survival rate was one year. 12 patients died during the analysis (86 %). From the whole number of treated patients 2 have survived (14 %) till nowadays. A female patient is 54 years old with AA gr. III has lived for 16 months since the treatment and another 42 years old patient with GBM has lived for 11 months since the treatment. Complications have appeared in two patients. In one case it was the inflammation of the skin in the place of fixed catheters antibiotic treatment. The second patient developed a postradiation cyst and an epileptic attack. The state of his health was stabilized after operation of the cyst. The survival rate after treatment did not improve in one patient, in other patients the survival rate had improved.

DISCUSSION

In spite of radical surgery, accurate planned and applied dose radiation, combined with chemotherapy, the state of patient@s health improved only minimall (35,36). In addition to low incidence of HG gliomas and short survival after the treatment, only in minimum patients with recurrent disease indicated further treatment. Statistical evaluation could not be performed due to small series of patients.

Zamboglou et al (8) applied intersticial BRT for patients with recurrent GBM. For all the patients had diagnose recurrent GMB from 6 to 60 months after primary treatment by external radiotherapy range 60 Gy. The second group were patients with solitary brain metastases. Age of patients was 23 to 73 (average 54.2 age) and the median tumour volume was 67 cm3 (range: 20- 114 cm^3). Keeping the constant geometry was used Perspex template without stereotactic framework. Every patient took part in 2 fractions BRT daily with the range of 5 Gy per fraction, totally TD 30-40 Gy, during 3 – 4 days. Survival rate was 42 weeks for 31 patients with AA and 29 weeks for 21 patients with GBM. Median survival rate of patients with solitary metastases was 50 weeks. Complications were appeared in 3 patients, 2 patients suffered lungs embolia and one developed meningitis. This study confirms the influence of IBRT to longer patients survival rate with minimum complications.

Between 1993 and 1997, 42 patients with recurrent glioblastoma were treated with implanted iridium 192 form in temporary implantation at the Salpetriere Hospital (1, 37). Treated tumour was (range:1.6 – 122 cm^3) with median tumour 23 cm^3. For 80 % was the survival rate 6 months, 48 % has lived for one year and 11 % has lived for 2 years. The median was 50 weeks. In 10 patients reoparation was done because of worse healts state with evident mass-effect. In 5 patients tumour was histologically confirmed, in 3 patients only by necrosis. The survival rate was not influenced by reoperation. Significant influence on the tumour size was confirmed – to 30 cm^3 and Karnofsky score over 70, on survival rate and the life quality of patients.

Radiation oncologists from the Elisabeth Hospital, Tiburg in Holland (38) published the results of curative treatment of 460 patients with HG gliomas. All the patients took part in biopsy or surgical removing of tumour brain tissue. Postoperated external radiotherapy was applied by 6 MeV photons in TD 60 Gy/30 fraction 5 times a week. 3 – 4 weeks after the last fraction ERT was done MR treatment. On the basis of selective criteria: the biggest range of tumour smaller than 50 mm, Karnofsky Performance status more than 70 %, tumour located supratentorially, aside critical structures (brain stem, motoric centre .....) was applied another radiation dose to patients into the tumour's tissue by the intersticial BRT form. As a source of radiation Ir 192 was used with the highest amount of catheters 14, all applied TD was 40 Gy in 10 fractions to TD 4.0 Gy twice a day. The median survival was 15 months against to 7 patients without brachytherapy. In patients with KI more than 70% the survival was 5 to 13 months against the patients with KI under 70 %. Complications after the operation were minimal. One patient developed an inflammation of the skin and 2 patients leaked liquor more than 24 hours. One patient did not finish the treatment

because of edema progress after 6 fractions BRT. This study confirms the reason of IBRT as a suitable method for supplementing of dose radiation, applied external radiotherapy.

D.C.Shrieveet with coworkers from Brain Tumor Center, Brigham and Women's Hospital in Bostone compare the efficacy of stereotactic rádiosurgery (SRS) and brachytherapy in the treatment of recurrent glioblastoma multiforme. The patients had either progressive GBM or pathologically proven GBM at recurrence after previous treatment for a lower grade astrocytoma. Thirty two patients were treated with interstitial brachytherapy, and 86 received treatment with stereotactic radiosurgery. The patient characteristics were similar in the two groups. Those patients treated with SRS had a median tumour volume of 10.1 cm^3 and received a median peripheral tumour dose of 13 Gy. Patients treated with brachytherapy had a median tumour volume of 29 cm^3. Median dose to the periphery of the tumour volume was 50 Gy delivered at a median dose rate of 43 cGy/hour. Median survival, measured from the time of treatment to recurrenece, in all patients treated with SRS was 10.2 months and the median surivival in all patients treated with brachytherapy was 11.5 months. A younger age and smaller tumour volume were predictive of better outcome.

Technical possibilities of stereotactic radiosurgery permit the treatment of tumour volume only to 10 cm^3, while the IBRT techniques do not have this limitation. Comparable benefit in surviving and the quality of patients' life after application of the both modalities definite advantages IBRT as the treatment appropriate even for the tumours of higher volume.

CONCLUSSION

Retreatment of malignant gliomas may be performed with palliative intent after careful consideration of the risks and benefits, and with special regards to iatrogenic neurotoxicity and quality of life (40).

Patients with recurrences AA and GMB, the reoperation does not have influence on patients surviving. Radicalization of reoperation is in the relation to the prognosis disputable (41). Benefit was recorded only in a group of patients with Karnofsky score above 90 (42). Reiradiation of operated on and not operated recurrences of HG gliomas by external radiotherapy is not indicated. It loads a big target volume of healthy brain tissue by radiation doses with the following functional changes and necrosis. Intersticial brachytherapy helps to apply treated dose of radiation with maximum preservation of surrounding tissue. Also the radiobiological research supported its importance. It confirms after IBRT the reduction of proliferated potencial live cells in tumour brain tissue (43, 44).

The optimalization of technical intersticial brachytherapy in recurrent HG gliomas at the OC MFN is in spite of a low amount of indicated cases well-founded in the world. Nowadays it is only one of possible methods of effective paliative treatment with quality benefit and the survival treated pacients rates.

REFERENCES

1. Mazeron JJ. Brain tumours. In: Gerbaulet A, Potter R, Mazeron JJ. The GEC ESTRO handbook of brachytherapy. Leuven, Belgium: ACCO; 2002. p. 585-591.
2. Suntharalingam N, Podgorsak EB, Tôlli H. Brachytherapy: Physical and clinical aspects. In: Podgorsak B. Review of radiation oncology physics: A handbook for teachers and students. Vienna: International atomic energy agency; 2004. p. 373-396.
3. Kleihues P, Cavenee WK. Pathology and Genetics of Tumours of the Nervous System. Lyon: IARC Press; 2000. p. 9-29.
4. Sneed PK, Gutin PH. Brachytherapy in central nervous system tumors. In: Leibel SA, Phillips TL. Textbook of radiation oncology. Philadelphia: B. Saunders Company; 1998. p. 371-382.
5. Suh JH, Barnett GH. Brachytherapy for brain tumor. Hematol Oncol Clin North Am 1999; 13: 635-650.
6. Šlampa P. a kol. Radiační onkologie v praxi. Brno: Masarykúv onkologický ústav; 2004. p. 143-155.
7. Simon JM, Cornu P, Boisserie G. Brachytherapy of gioblastoma recurring in previoustly irradiated territory: predictive value of tumor volume. Int J Radiat Oncol Biol Phys 2002; 53: 67-74.
8. Jansen E, Dewit L, van Herk M. Target volumes in radiotherapy for high-grade malignant glioma of the brain. Radiother Oncol 2000; 56: 151-15.
9. Zamboglou N, Kolotas Ch, Baltas. Clinical evaluation of CT based software in treatment planning for intersti-

tial HDR brachytherapy. In: Speiser BL, Mould RF. Brachytherapy for the 21st century. Veenendaal: Nucletron B.V.; 1998. p. 321-327.
10. Shafman TD, Loeffler JS. Novel radiation technologies for malignant gliomas. Curr Opin Oncol 1999;11: 147-151.
11. Sneed PK, McDermott MW, Gutin PH. Interstitial brachytherapy procedures for brain tumors. Semin Surg Oncol 1997; 13: 157-166.
12. Chin HW, Bahrass F, Davis P. Modern therapeutic approach for high grade astrocytoma: intracranial Ir-192 brachytherapy. J La State Mes Soc 1991; 143: 33-36.
13. Kala M. Maligní nádory mozku dospělého věku. Praha: Galén; 1998. p. 9-53.
14. Gross MW, Webwe WA, Feldmann HJ. The value of F-18-fluorodeoxyglucose PET for the 3-D radiation treatment planning of malignant gliomas. Int J Radiat Oncol Biol Phys 1998; 41: 989-995.
15. Nori D, Parikh S. Intraoperative brachytherapy. In: Speiser BL, Mould RF. Brachytherapy for the 21st century. Veenendaal: Nucletron B.V.; 1998. p. 292-299.
16. International Commission on Radiation Units and Measurement: ICRU Report 50. Prescribing, recording and reporting photon beam therapy. Bethesda, Maryland; 1993.
17. International Commission on Radiation Units and Maesurement: ICRU Report 62. Supplemetum to ICRU 50. Bethesda, Maryland; 1999.
18. International Commission on Radiation Units and Measurement: ICRU Report 58. Dose and volume specification for reporting interstitial therapy. Bethesda, Maryland; 1997.
19. Brada M, Bidmead M. Geometric uncertainties in radiotherapy of the brain. London: Published by The British Institute of Radiology; 2003. p. 109-125.
20. Khoo VS, Dearnaley DP, Finnigan DJ. Magnetic resonance imaging (MRI): considerations and applications in radiotherapy treatment planning. Radiother Oncol 1997; 42: 1-15.
21. Cejpek P, Krupa P, Štourač P. Maligní nádory mozku. In: Adam Z, Vorlíček J, Vaníček. Diagnostické a léčebné postupy u maligních chorob. Praha: Grada; 2004. p. 13-26.
22. Schiffer D. Brain tumors biology, pathology and clinical references. Berlin:Springer-Verlag; 1997. p. 137-213.
23. Vaníček J, Krupa P.: Využití zobrazovacích metod pro diagnostiku maligních chorob. In: Adam Z, Vorlíček J, Koptíková J. Obecná onkologie a podpúrná léčba. Praha: Grada; 2003. p. 155-186.
24. Schultheiss TE, Kun LE, Ang KK. Radiation response of the central nervous system. Int J Radiat Oncol Biol Phys 1995; 31: 1093-1112.
25. Chang J, Thakur G, Perera G. Image-fusion of MR spectroscopyic images for treatment planning of gliomas. Int J Radiat Oncol Biol Phys, supplement 1, 2004; 60: S223-S224.
26. Pirzkall A, McKnight TR, Graves EE. MR-spectroscopy giuded target delineation for high-grade glioma. Int J Radiat Oncol Biol Phys 2001; 50: 915-928.
27. Kolotas C, Baltas D, Zamboglou N. CT-Based interstitial HDR brachytherapy. Strahlenter Onkol 1999; 175: 419-427.
28. Aird EG, Wiliams JR, Rembowska A. Brachytherapy. In: Williams JR, Thwaites DI. Radiotherapy Physics in Practice. New York: Oxford University Press; second edition 2000. p. 247-288.
29. Smith AR. Radiation Therapy Physics. Berlin: Springer-Verlag; 1995. p. 247-303.
30. Vigneron D, Bollen A, McDermott LW. Three-dimensional magnetic resonance spectroscopic imaging of histologically confirmed brain tumors. Magnetic resonance imaging 2001; 19: 89-101.
31. Pirzkall A, Li X, Oh, J. 3D MRSI for resected high-grade gliomas before RT. Tumor extent according to Metabolic activity in relation to MRI. Int J Radiat Oncol Biol Phys 2004; 59: 126-137.
32. Ishikawa M, Kikuchi H, Miytake S. Glucose consumption in recurrent gliomas. Neurosurgery 1993; 33: 28-33.
33. Rosalie J, Terence Z, Coleman RE. Positron emission tomografy: Brain tumors and lung cancer. Radiol Clin 2001; 39: 871-881.
34. Bělohlávek O, Jarúšková M, Šimonová K. Atlas of Positron Emission Tomography. Praha: Lacomed; 2004, 10-21.
35. Grossman SA, Batara J. Current management of glioblastoma multiforme. Semin Oncol 2004; 31: 635-644.
36. Jurga Ľ, Malý M. Úvahy o úskaliach kombinovanej liečby nádorov glie. Klin Onkol 2007; 2: 227-230.
37. Boisserie G, Cornu P, Sahel M. Iridium192 brachytherapy of supratentorial high grade glioma recurring in irradiates areas: technique and preliminary results of the Pitié-Salpetiere hospital group. Bull Cancer Radiother 1996; 83: 144-152.
38. Gutin PH, Prados MD, Phillips TL. External irradiation followed by an interstitial high activity implant boost in the initial treatment of malignant gliomas. Int J Radiat Oncol Biol Phys 1991; 21: 601-606.
39. Shrieve DC, Alexander E, Wen PY. Comparison of stereotactic radiosurgery and brachytherapy in the treatment of recurrent glioblastoma multiforme. Neurosurgery 1995; 36: 275-282.
40. Nieder C, Grosu A, Molls M. A comparison of treatment results for recurrent malignant gliomas. Cancer Treat Rev 2000; 26: 397-409.
41. Abrey LE, Mason WP. Brain tumors. Oxford: Health Press; 2003. p. 56-65.
42. Pinsker M, Lumenta C. Experiences with reoperation on recurrent glioblastoma multiforme. Zentralbl Neurochir 2001; 62, 43-47.
43. Steel G. Basic clinical radiobiology, 3rd edition. London:Arnold; 2002. p. 192-204.
44. Kunishio K, Matsumoto K, Higashi H. Proliferative potential of malignant glioma cells before and after interstitial brachytherapy. Neurol Med Chir 1999; 39: 341-349.

Received: March, 12, 2008
Accepted:May, 30, 2008

CONTENT VALIDATION OF HOPELESSNESS IN SLOVAKIA

KATARÍNA ŽIAKOVÁ, JURAJ ČÁP, ELENA GURKOVÁ
Institute of Nursing, Comenius University in Bratislava, Jessenius Faculty of Medicine in Martin, Slovak Republic

A b s t r a c t

The aim of this study was to examine the validity of nursing diagnosis *Hopelessness* and to identify the related defining characteristics in Slovak social and cultural context. A qualified sample of 17 nurses and 18 university teachers was given measuring instrument consisting of 15 NANDA characteristics, 17 *Nowotny Hope Scale* characteristics and 4 fictitious characteristics. From 36 characteristics 12 reached the value of weighted average of the scores for defining characteristics (0.70). Only 2 NANDA characteristics have reached the value 0.70. Results of the study confirm that defining characteristics of the diagnosis *Hopelessness* are in NANDA taxonomy defined ambiguously**.** The characteristics that reached high importance can be prioritized for the use in clinical practice to identify the patient's hopelessness and make a diagnosis.

Key words: Hopelessness, NANDA International, content validation

INTRODUCTION

Classification of nursing diagnoses together with their diagnostic characteristics, their clinical use and reflection of social-cultural differences are the basic presumptions of use of the terminology in international context. International validation studies can provide a basis for this effort. Diagnostic content validation of nursing diagnoses is a recommended means to confirm the defining characteristics necessary to establish a specific nursing diagnosis. The diagnostic content validity model has been used in numerous studies to develop lists of defining characteristics recommended by experts as being present in patients with specific diagnoses.

Trying to interconnect theoretical bases with practice, we have decided to pay attention to validation of the nursing diagnosis Hopelessness. The defining characteristics of diagnosis on NANDA's list are used by nurses to identify accurate diagnoses. The defining characteristics of hopelessness, however, were not previously validated for use in Slovakia. Hoplessness is defined „as subjective state in which individual sees limited or no alternatives or personal choices available and is unable to mobilize energy on own behalf" (1) and it has 12 defining characteristics. We used the modified Fehring's Diagnostic Content Validity Model (DCV) (5) and created a validation form to assess diagnostic characteristics of the diagnosis Hopelessness.

METHODS

Developing the validation form

Validation form involved 36 diagnostic characteristics that were created from three groups. The first group consisted of diagnostic characteristics of the diagnosis Hopelessness (code 00124) of NANDA (2) (see Table 1). Coming from the experience of Wake, Fehring and Fadden (3), who added also the characteristics of standard measuring instruments, we included into the study another group of diagnostic characteristics (See Table 1) taken over from Nowotny Hope Scale – further as NHS (4). The list was completed with four fictitious characteristics (see Table 1).

A d d r e s s f o r c o r r e s p o n d e n c e:
Assoc. Prof. Katarína Žiaková, MSc, PhD., Institute of Nursing, Comenius University in Bratislava, Jesseniuss Faculty of Medicine in Martin, Malá Hora 5, 036 32 Martin, Slovakia
e-mail:ziakova@jfmed.uniba.sk

Table 1 Diagnostic Characteristics of *Hopelessness*

Diagnostic Characteristics of NANDA Taxonomy II	Diagnostic Characteristics on the Base of NHS	Fictitious Diagnostic Characteristics
No initiative	Lack of trust of own abilities	Perspiring
Turning away from the speaker, shrugging as response taciturnity	Lack of activity	Loss of appetite
Lack of interest in close people	Inability to act	Tremble in limbs
No involvement in care	Inability to learn	Draught in mouth
Overall passivity	Inability to change anything	
Passive care accepting	Inability to accept changes	
Belief that the problems will always be here	Inability to adapt	
Belief that nothing will change	Distrust of result	
Cumbersome slow thinking	Distrust of help	
Indecision	Inability to plan future	
Expressing helplessness, sighs	Inability to make decisions	
Expressions like „i cannot“	Distrust of own strengths	
Expressions without emotional demonstration	Distrust of own abilities	
Outbursts of anger and aggressiveness	Experience of loneliness	
Closing eyes/avoiding eye contact	Belief there is nobody to turn to	
	Belief there is nobody to consult	
	Troubles with aiming targets and plans for future	

Using Diagnostic Content Validity Model (5), experts determined the degree of importance of a characteristic on the Likert's scale in relation to the diagnosis Hopelessness (code 00124). Single levels of the scale mean: 5 - the highest importance, 4 - high importance, 3 - medium importance, 2 - little importance, 1 - no importance.

Subjects and sampling

The sample for the validation study consisted of people with appropriate experience of hopelessness. We selected a number of experts to validate the importance of diagnostic characteristics. The experts were university teachers and nurses with minimum higher special education and five-year experience in the area (6). The sample was comprised of 18 university teachers (Department of Nursing at Jessenius Medical Faculty in Martin) and 17 nurses (Martin Faculty Hospital). Total number of respondents involved into the study was n = 35. The mean age of nurses was 37.8 (± 8.6) years with 19.06 (± 8.6) years of experience. The mean age of teachers was 34.4 (± 9.7) years with 11.8 (± 9.9) years of experience.

Data collection

The experts completed a validation survey form during 5 sessions at the Department of Nursing Jessenius Medical Faculty in Martin between January and March 2007.

Statistical analyses

Statistical analyses were performed in Statgraphics (V.5.0.). Descriptive statistics (including means, standard deviations, weighted average of the scores) were calculated. The weighted average of the scores was calculated based on the arithmetic mean by assigning

the weight of 1 to the level of 5 (the highest importance) and the weight of 0 to the level of 1 (no importance). Thus for the level 4 the corresponding weight is 0.75, for level 3 weights 0.5 and for level 2 the corresponding weight is 0.25. During the study we also identified correlation between single defining characteristics by calculation of a single linear correlation (Pearson's correlation coefficient). The level of critical statistical importance of this correlation (p) was also identified.

RESULTS

Validation of Defining Characteristics

Based on the analysis of the answers of experts we identified defining diagnostic characteristics for the nursing diagnosis of hopelessness (see Table 2). Single characteristics are listed by the importance up to the level of the weighted average of scores 0.70.

From the total number of 36 presented characteristics, following 10 can be considered

Table 2 Defining Characteristics of Hopelessness

Characteristic	X ± SD	WAS*
35 belief there is nobody to turn to	4.17 ± 0.95	0.79
36 belief there is nobody to consult	4.11 ± 0.99	0.78
26 distrust of result	4.03 ± 0.71	0.76
37 troubles with aiming targets and plans for future	4.03 ± 0.75	0.76
7 overall passivity	4.03 ± 0.92	0.76
27 distrust of help	3.94 ± 0.87	0.74
23 inability to change anything	3.91 ± 0.89	0.73
28 inability to plan future	3.86 ± 0.88	0.72
31 distrust of own strength	3.83 ± 0.82	0.71
34 experience of loneliness	3.83 ± 0.98	0.71
29 inability to make decisions	3.8 ± 0.83	0.7
10 belief that nothing will change	3.8 ± 0.99	0.7

*WAS: Weighted average of the scores

defining: belief that there is nobody to turn to (0.79), belief that there is nobody to consult (0.78), distrust of the result (0.78), troubles with aiming targets and plans for future (0.75), overall passivity (0.76), distrust of help (0.74), inability to change anything (0.73), inability to make plans for future (0.72), distrust of own strengths (0.71), experience of loneliness (0.71), inability to make decisions (0.7), belief that nothing will change (0.7).

From NANDA diagnostic characteristics for the diagnosis Hopelessness the respondents listed in defining diagnostic characteristics the following ones: overall passivity (0.76) and belief that things will not change (0.7), which means that of the presented 15 characteristics the respondents consider as defining only 2 characteristics.

From the characteristics based on NHS items, following were determined as defining: belief that there is nobody to turn to (0.79), belief that there is nobody to consult (0.78), distrust of the result (0.78), troubles with aiming targets and plans for future (0.76), distrust of help (0.74), inability to change anything (0.73), inability to make plans for future (0.72), distrust of own strengths (0.71), experience of loneliness (0.71), inability to make decisions (0.7).

From the presented fictitious characteristics: perspiring, loss of appetite, tremble in limbs and draught in mouth, not a single one was included into the group of defining characteristics by respondents.

DISCUSSION

The characteristics created by single NHS items were judged by experts as to be more important for the diagnosis Hopelessness which is confirmed by the ratio of characteristics between NANDA/NHS (2:10). Diagnostic characteristics found defining by nurses were aimed mostly to an individual, his or her active participation and inside activity (overall passivity, no initiative, distrust of the result, distrust of own abilities). Teachers involved into defining characteristics a group expecting help and social support from other people (belief there is nobody to turn to, belief there is nobody to consult) and characteristics aimed to planning and expected results (troubles with aiming targets and plans for future, inability to make plans for future).

All mentioned correlations are positive, moving in the range of 0.35 to 0.69 which responds to moderate up to strong correlation. The strongest correlations were between the characteristics 35 and 36, 26 and 27, 28 and 29. The correlations can be covered by a fact that some characteristics are ascribed by one factor or they can show a connection between characteristics (See Table 3). For example, if a patient does not believe in the result, we can also suppose that he or she is sure they cannot change anything. Such connections are important for finding conclusions in clinical practice and it would be appropriate to verify them in it.

Sato (7) validated twelve nursing diagnoses of NANDA in Japanese social and cultural context on the sample of 214 experts. He found out that in the diagnosis Hopelessness there were not found any diagnostic characteristics of the value of weighted average of the scores of defining characteristics.

Wake, Fehring and (3) in their multiethnic study tested three nursing diagnoses: Hopelessness, Anxiety and Ineffective Cleaning of Airways. The study was run in six countries on the sample of 236 nurses specialized in intensive care. Common defining characteristics were identified only for the diagnosis Anxiety and Ineffective Cleaning of Airways. For the diagnosis Hopelessness, no characteristics reached the value of weighted average of the scores for defining characteristics.

In our study, only two NANDA characteristics have reached the value of weighted average of the scores for defining characteristics. This difference can be caused by relatively lower sample of experts participating in the study and the fact that for our social and cultural context, we have decided to use the bottom limit of the value of weighted average of the scores of defining characteristics (0.70) used with the DCV model.

Table 3 Correlation among Defining Characteristics

Name of diagnostic characteristic	26 distrust of result	27 distrust of help	28 inability to plan future	29 inability to make decisions	34 experience of loneliness	35 belief there is nobody to turn to
10 Belief that nothing will change		r = 0.43*	r = 0.4*		r = 0.41*	
23 Inability to change anything	r = 0.43**					r = 0.43**
27 Distrust of help	r = 0.67***					
29 Inability to make decisions			r = 0.6***			
31 Distrust of own strengths			r = 0.37*			
35 Belief there is nobody to turn to					r = 0.35*	
36 Belief there is nobody to consult						r = 0.69***
37 Troubles with aiming targets and plans for future				r = 0.39*		

$p < 0.05^{*}$ $p < 0.005^{**}$ $p < 0.0005^{***}$

From NHS characteristics, only ten reached the value of weighted average of the scores for defining characteristics. Results of our validation study as well as results of above mentioned studies confirm the fact that defining characteristics of diagnosis Hopelessness are in NANDA taxonomy defined ambiguously. That creates doubts about their relevance in relation to diagnosis Hopelessness in clinical practice. More items (10) selected of NHS reached the value of weighted average of the scores to 0.70. We think that higher scores of these items is caused by the fact that the NHS tool went through the process of validation that unambiguously confirmed the relation of its single items to the phenomenon of hope even in our social and cultural context (4).

Some characteristics defined by NANDA taxonomy (e.g. shrugging, turning away from the speaker, cumbersome slow thinking, expressions like „I cannot“, expression without emotional demonstration, outbursts of anger and aggressiveness, closing eyes/avoiding eye contact, slow respond to stimulus) can not be considered specific to the diagnose Hopelessness compared with basic NHS subscales (belief in result, relations with others, what we hope is possible, faith, inside activity, commitment).

The use of NANDA International provokes discussions among teachers, nurses, even students. The most often criticism is aimed to the terminology of diagnoses and wide definiti-

on of their diagnostic characteristics which are difficult to verify. Another problem is that they are unrepresentative e.g. some characteristics of NANDA taxonomy are determined as defining for diagnoses Hopelessness, Anxiety and Fear. We have also found a problem when a diagnosis determined independently (e.g. Hopelessness) is a defining characteristic of other diagnoses (e.g. hopelessness as a diagnostic characteristic for diagnoses Anxiety, Anticipatory grieving, Helplessness). In professional literature there can also can be found various modifications of determination of defining characteristics for single NANDA diagnoses (8) that try to solve the problem but lack a uniform basis (at least uniformity in determination of defining characteristics).

CONCLUSION

The result of the study is a hierarchical set of diagnostic characteristics in relation to the diagnosis Hopelessness. The hierarchical set was created according to validation methods and its aim was to select characteristics significant in Slovak social and cultural context. The characteristics that reached high importance can be prioritized for the use in clinical practice to identify the patient's hopelessness and make a diagnosis.

REFERENCES

1. Nursing diagnoses : Definitions & Classification 2007-2008. Philadelphia: NANDA International; 2007.
2. Doenges, ME., Moorhouse, MF. Kapesní průvodce zdravotní sestry. Praha: Grada Publishing; 2001.
3. Wake, MM., Fehring, RJ., Fadden, T. Multinational validation of anxiety, hopelessness and ineffective airway clearance. 1991; 2: 57-65.
4. Nowotny, ML. Assessment of hope in patient with cancer: Development of an instrument. Oncology Nursing Forum 1989; 16 (1): 57-61.
5. Fehring, RJ. Validating diagnostic labels: Standardized methodology. Classification of Nursing Diagnoses: Proceedings of the sixth conference. M.E. Hurley (ed.), Mosby, St. Louis 1986: 39-49.
6. Whitley, GG. Processes and methodologies for research validation of nursing diagnoses. Nursing Diagnosis 1999 10: 5-14.
7. Sato, S. Diagnostic concept development: Content validation of North American nursing diagnoses in Japan. Digital Dissertation, (UMI No. 9707888). Available at http://wwwlib.umi.com/dissertations/fullcit/9707888 (accessed 12 december 2002).
8. Creason, SN. Clinical validation of nursing diagnoses. International Journal of Nursing Terminologies and Classifications 2004; 15:123-132

Acknowledgement: This work was supported by research project VEGA No. 1/2484/05.
Received: April, 15, 2008
Accepted: May, 30, 2008